Selective Extraction of Uranium from Liquid or Supercritical Carbon Dioxide

Fuel Cycle Research & Development

Prepared for
U.S. Department of Energy
Fuel Cycle Research & Development
Anne F. Farawila
Matthew J. O'Hara
Harry Z. Taylor
Chien M. Wai
Yu-Jung Liao

Pacific Northwest National Laboratory
University of Idaho

July 31st 2012
PNNL-21590

Reviewed by:

Director, Fuel Cycle Research and Development

Andy Griffith Date

Concurred by:

Director, FCT Technical Integration Office

Phillip Finck Date

Approved by:

Deputy Assistant Secretary, Fuel Cycle Management

(FCT Program Manager) Monica Regalbuto Date

SUMMARY

Current liquid-liquid extraction processes used in recycling irradiated nuclear fuel rely on (1) strong nitric acid to dissolve uranium oxide fuel, and (2) the use of aliphatic hydrocarbons as a diluent in formulating the solvent used to extract uranium. The nitric acid dissolution process is not selective. It dissolves virtually the entire fuel meat which complicates the uranium extraction process. In addition, a solvent washing process is used to remove TBP degradation products, which adds complexity to the recycling plant and increases the overall plant footprint and cost.

A liquid or supercritical carbon dioxide (l/sc -CO_2) system was designed to mitigate these problems. Indeed, TBP nitric acid complexes are highly soluble in l/sc -CO_2 and are capable of extracting uranium directly from UO_2, UO_3 and U_3O_8 powders. This eliminates the need for total acid dissolution of the irradiated fuel. Furthermore, since CO_2 is easily recycled by evaporation at room temperature and pressure, it eliminates the complex solvent washing process.

In this report, we demonstrate:

(1) A reprocessing scheme starting with the selective extraction of uranium from solid uranium oxides into a TBP-HNO_3 loaded Sc-CO_2 phase,
(2) Back extraction of uranium into an aqueous phase, and
(3) Conversion of recovered purified uranium into uranium oxide.

The purified uranium product from step 3 can be disposed of as low level waste, or mixed with enriched uranium for use in a reactor for another fuel cycle.

After an introduction on the concept and properties of supercritical fluids, we first report the characterization of the different oxides used for this project. Our extraction system and our online monitoring capability using UV-Vis absorbance spectroscopy directly in sc-CO_2 is then presented. Next, the uranium extraction efficiencies and kinetics is demonstrated for different oxides and under different physical and chemical conditions: l/sc -CO_2 pressure and temperature, TBP/HNO_3 complex used, reductant or complexant used for selectivity, and ionic liquids used as supportive media. To complete the extraction and recovery cycle, we then demonstrate uranium back extraction from the TBP loaded sc-CO_2 phase into an aqueous phase and the characterization of the uranium complex formed at the end of this process.

Another aspect of this project was to limit proliferation risks by either co-extracting uranium and plutonium, or by leaving plutonium behind by selectively extracting uranium. We report that the former is easily achieved, since plutonium is in the tetravalent or hexavalent oxidation state in the oxidizing environment created by the TBP-nitric acid complex, and is therefore co-extracted. The latter is more challenging, as a reductant or complexant to plutonium has to be used to selectively extract uranium. After undertaking experiments on different reducing or complexing systems (e.g., AcetoHydroxamic Acid (AHA), Fe(II), ascorbic acid), oxalic acid was chosen as it can complex tetravalent actinides (Pu, Np, Th) in the aqueous phase while allowing the extraction of hexavalent uranium in the sc-CO_2 phase.

Finally, we show results using an alternative media to commonly used aqueous phases: ionic liquids. We show the dissolution of uranium in ionic liquids and its extraction using sc-CO_2 with and without the presence of AHA. The possible separation of trivalent actinides from uranium is also demonstrated in ionic liquids using neodymium as a surrogate and diglycolamides as the extractant.

CONTENTS

FIGURES

TABLES

ACRONYMS

AHA	AcetoHydroxamic Acid
CO_2	Carbon dioxide
DOE	Department of Energy
FCR&D	Fuel Cycle Research & Development
HLW	High Level Waste
HNO_3	Nitric Acid
H_2O	Water
LLW	Low Level Waste
l/sc-CO_2	Liquid or Supercritical CO_2
MOC	Modified Open Fuel Cycle
MOX	Mixed OXides
MW	Molecular Weight
NE	Nuclear Energy
P_c	Critical pressure
PNNL	Pacific Northwest National Laboratory
Pu	Plutonium
SFE	Supercritical Fluid Extraction
sc-CO_2	Supercritical CO_2
TBP	Tributyl Phosphate
T_c	Critical temperature
U	Uranium
UO_2	Uranium dioxide
UO_3	Uranium trioxide
U_3O_8	Triuranium octoxide
UV-Vis	Ultra-Violet and Visible

FUEL CYCLE R&D PROGRAM
Separations and Waste Form

1. INTRODUCTION

This report shows the progress made by PNNL and the University of Idaho on the Fuel Cycle R&D program between June 2011 and July 2012. In this report, we demonstrated a reprocessing scheme starting with the selective extraction of uranium oxides into a TBP-HNO_3 loaded sc-CO_2 phase, the back extraction of uranium into an aqueous phase and its recovery as uranium oxide. The process limits proliferation risks, as the plutonium is either co-extracted with the uranium or left behind with the fission products. The process also allows the recovery of uranium that could be disposed of as low level waste to significantly reduce the volume of high level waste, or used as Mixed OXides (MOX) fuel, or mixed with enriched uranium for use in a reactor for another fuel cycle.

In the introduction, the concept bases and advantages are first described followed by a background overview on supercritical fluids and an overview of the ability of supercritical CO_2 (sc-CO_2) to extract uranium. The characteristics of several uranium oxides (UO_2, U_3O_8, UO_3) used in our extraction system are shown in the next section. This characterization was essential to calibrate the UV-Vis online monitoring spectrometer in order to assess $UO_2(NO_3)_2(TBP)_2$ complex solubility and determine uranium extraction efficiencies of the different oxides in sc-CO_2. UV-Vis Spectrometer calibration, uranium solubility and extraction efficiency are three steps described in the following sections. Next, to complete our reprocessing scheme, we demonstrated uranium back-extraction into an aqueous phase and its reconstitution into an oxide. The inhibition of plutonium extraction in the presence of reducing or complexing agents was then shown. Finally, results using ionic liquids, instead of more common aqueous chemistry, as a supportive media for the selective extraction of lanthanides and actinides will be presented.

1.1 Concept Basis

For this project, we proposed to evaluate the selective dissolution and extraction of uranium from irradiated nuclear fuel using extractant-loaded liquid or supercritical CO_2. This concept could revolutionize the nuclear fuel reprocessing industry by substantially simplifying the extraction and purification of uranium to enable Modified Open fuel Cycles (MOCs, now called limited recycle approach). A proposed schematic for irradiated fuel reprocessing using liquid or supercritical carbon dioxide (l/sc-CO_2) as a solvent is shown in Figure 1. The uranium extractant (e.g., TBP/HNO_3 complex) and possibly a plutonium reductant or ligand (e.g., acetohydroxoxamic acid, AHA) used to avoid plutonium and uranium co-extraction, are totally dissolved in CO_2, making the initial dissolution of uranium (and its other fuel components) in nitric acid unnecessary. This method readily recovers the valuable uranium component of the fuel for recycle or LLW disposal, thereby significantly reducing high level waste volume. The process would be a key enabling feature of many MOCs.

1.2 Concept Advantages

Current liquid-liquid extraction processes used in recycling irradiated nuclear fuel rely on (1) strong nitric acid to dissolve uranium oxide fuel, and (2) the use of aliphatic hydrocarbons as a diluent in formulating the solvent used to extract uranium. The nitric acid dissolution process is not selective. It dissolves virtually the entire fuel meat, including fission products and transuranics, which complicates the uranium extraction process and adds to the radiological dose of the uranium purification process. In addition, a solvent washing process is used to remove TBP degradation products,[1] which adds complexity to the recycling plant and increases the overall plant footprint and cost.

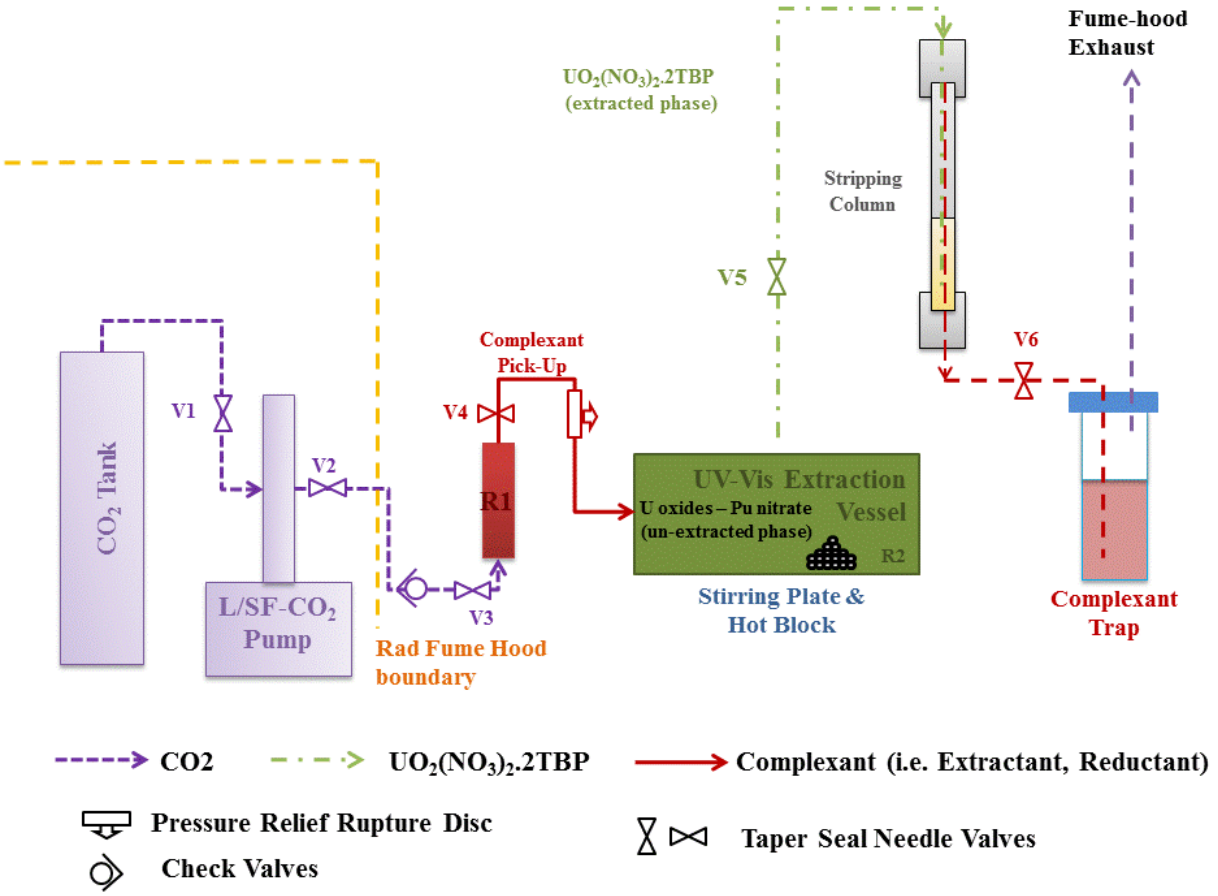

Figure 1. Schematic of the SFE system with stripping column

A l/sc-CO_2 system can be designed to mitigate these problems. Indeed, TBP nitric acid complexes are highly soluble in CO_2[2] and are capable of extracting uranium directly from UO_2, UO_3 and U_3O_8 powders in l/sc-CO_2. [3-6]Carrot, Wai and coworkers have shown that uranium solubility in a TBP/HNO_3/sc-CO_2 system can approach levels of 0.45 mol/L uranium (~100 g/L U).[7] Because nitric acid is only used in the TBP complexes to oxidize U(IV) and make uranium available for extraction by forming $UO_2.(NO_3)_2$, the proposed system eliminates the need for total acid dissolution of the irradiated fuel. This one step dry extraction process will therefore reduce acidic waste streams and, since CO_2 is easily recycled by evaporation at room temperature and pressure, it eliminates the complex solvent washing process. In addition, promising uranium decontamination factors (>10^3) from fission products were reported by Shimada et al.,[8] and the Japan Atomic Energy Agency is pursuing a direct (acid dissolver free) extraction process called Super-DIREX.[9] However, plutonium and neptunium are co-extracted with uranium in those processes. We propose to simplify the separation processes by selectively extracting uranium for MOCs.

As with pressurized water reactors that operate at similar pressures (150 bars) and higher temperatures (300 °C) than supercritical CO_2 systems, with proper engineering and administrative controls, extremely safe high pressure reprocessing systems can be created. sc-CO_2 extraction is safely and routinely used at industrial scales. One example of the nuclear industrial use of sc-CO_2 includes the recovery of uranium from incinerator ash[3] (AREVA in Richland, WA). For nuclear application, safety can be maximized and the consequences of an incident can be minimized by implementing rigorous designs, procedures, and engineering controls such as (1) secondary containment, (2) pressure relief valves, and (3) small batch volumes.

2. PROPERTIES OF SUPERCRITICAL FLUIDS, CO_2 SPECIFICALLY

A fluid is called supercritical when both its temperature and pressure exceed their critical values (T_c for the critical temperature and P_c for the critical pressure). A phase diagram for CO_2 is shown in Figure 2 with a representation of the supercritical and the subcritical region.

Different fluids such as water, methanol, ammonia, etc. can be in the supercritical state. Supercritical CO_2 offers numerous advantages over the other fluids: it has moderate critical values (T_c=31.1°C and P_c=1070 PSI), and it is inert, nontoxic, nonflammable, inexpensive and widely available in purified form. Furthermore, it is a gas at normal temperature and pressure, allowing an easy recovery of the extracted species without generation of secondary wastes that are very hard to discard or reprocess. These characteristics made CO_2 the most widely used substance for supercritical fluid applications.

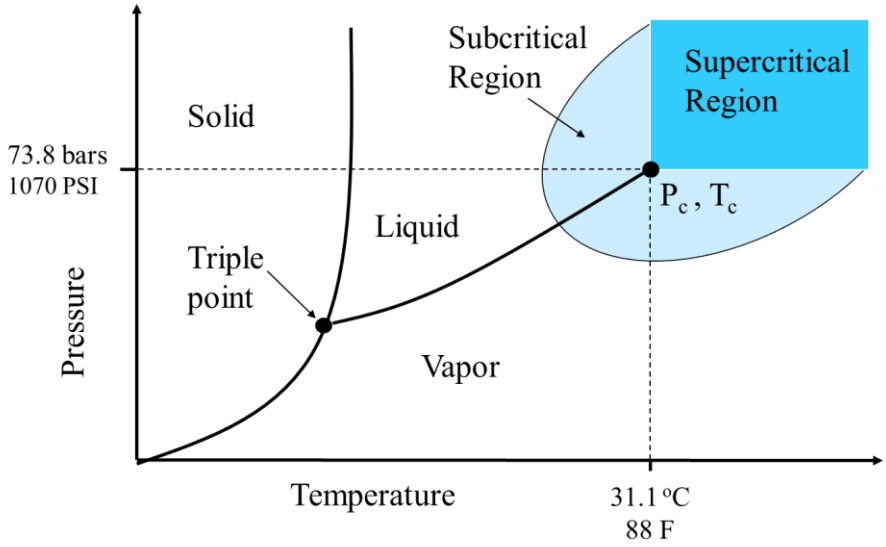

Figure 2. Phase diagram for CO_2

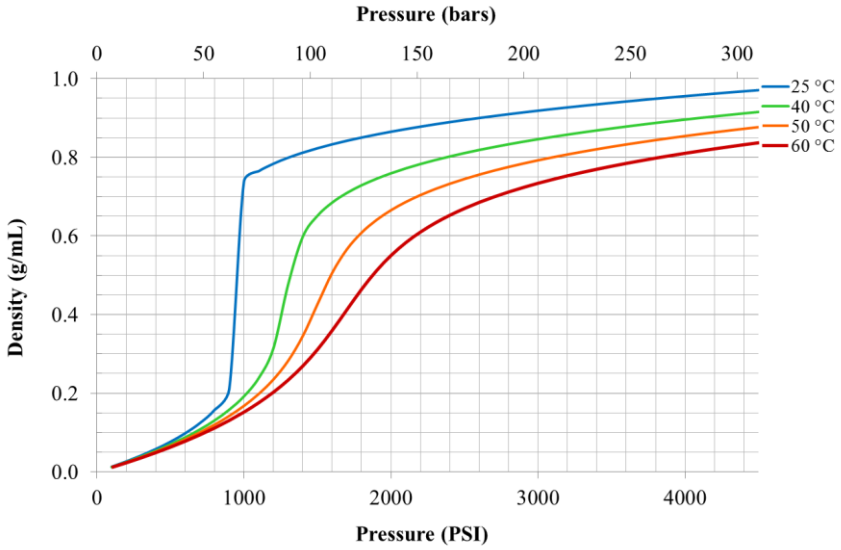

Figure 3. CO_2 density dependence on pressure and temperature. Data from NIST webbook: http://webbook.nist.gov/chemistry/fluid/

Supercritical fluid density depends on pressure and temperature. See Figure 3 for CO_2. The density of a fluid increases with pressure and decreases with an increase in temperature. The solubility of a substance in sc-CO_2 is related to its density and temperature. Solubility increases with an increase in density at constant temperature and decreases with increasing temperature at constant pressure.

Near the critical point, it is not unusual to observe inconsistency in density or other physical properties. The system can be greatly disturbed by a small difference in temperature or pressure or by adding a substance or an impurity to the fluid. It is then important to avoid quantitative measurements in the neighborhood of the critical values (T_c,P_c).

3. URANIUM OXIDES CHARACTERIZATION

Three uranium oxide powders, UO_2, UO_3, and U_3O_8, were purchased from International Bio-Analytical Industries Inc. (ibilabs, Boca Raton, Fl) to explore U dissolution in l/sc-CO_2. The supplier gave us an estimate of mesh size, as well as the isotopics and properties, as summarized in Table 1.

Table 1. Uranium oxide characteristics given by supplier (ibilabs)

Chemical Formula	Molecular weight ($g.mol^{-1}$)	U properties, Isotopics	Mesh size (mesh)	Calculated diameter (µm)
UO_2	270.03	Depleted	>325, <100	Between 44 and 149
UO_3	286.03	Natural	<100	Less than 149
U_3O_8	842.09	Depleted	400	Less than 37

However, alpha energy spectroscopy, as seen in Figure 4, revealed that U_3O_8 has natural uranium while UO_3 and UO_2 are depleted. For natural uranium, the U-238/U-234 peak ratio is close to 1 because over time the two isotopes reach a secular equilibrium. If the Uranium is depleted, the U-234 peak is generally reduced (~10% the activity of U-238), as U-234 is separated with U-235 in the enrichment process. In our UO_2 and UO_3 spectra (Figure 4a & 4c), the small U-234 peak contribution indicates that UO_2 and UO_3 are depleted. However, the U-234 peak for the U_3O_8 spectra (Figure 4b) is approximately half the activity of the U-238 peak indicating that this oxide contains some natural uranium. The supplier was informed of the error and is looking into understanding the discrepancy.

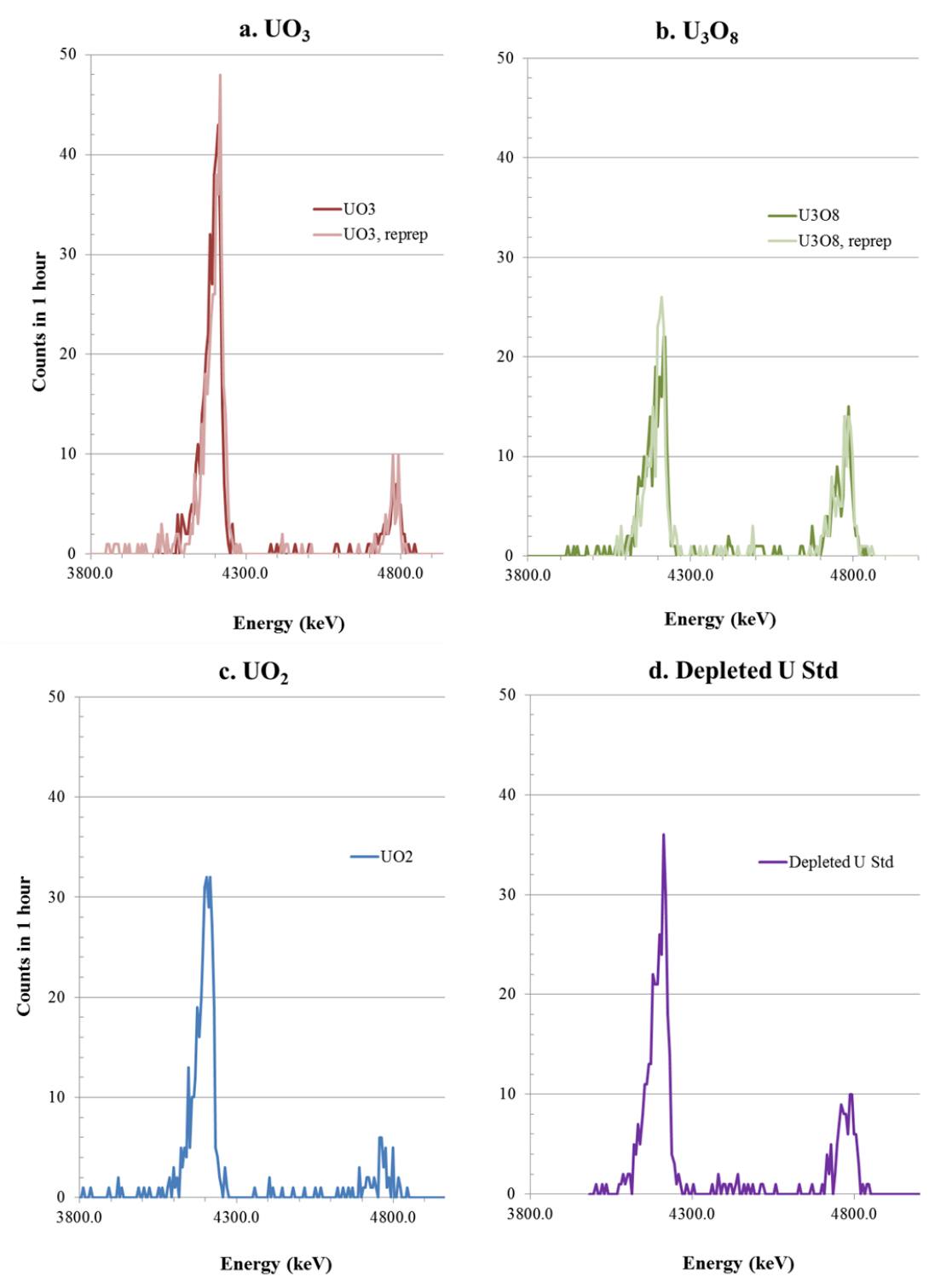

Figure 4. Alpha spectra of the oxides used (a. UO_3, b. U_3O_8, and c. UO_2) and of a depleted uranium standard of 0.25% U-235 (d.). U-238 peaks are at 4210 keV and U-234 peaks at 4775 keV.

We also determined the particle size distribution for the three oxides as this factor has an influence on dissolution rates and possibly the extraction efficiency. Figure 5 shows the particle size distribution obtained with a Hydro 2000µP micro-volume wet sample dispersion unit (Malvern Instruments Ltd, Malvern, UK). Actual values for different percentiles are shown in Table 2 with the specific surface area measured using the particle size distribution and BET measurements.

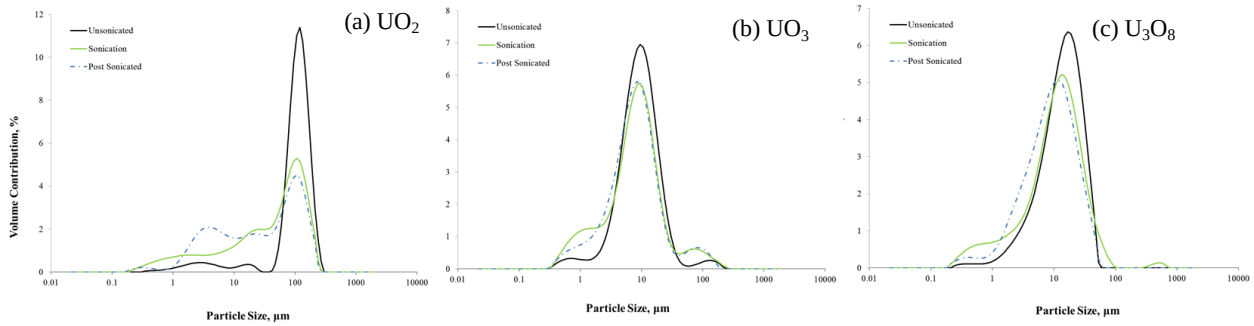

Figure 5. Particle size distribution for a. UO_2, b. UO_3, and c. U_3O_8

Table 2. Particle size and specific surface area for UO_2, UO_3, and U_3O_8

	Unsonicated			Sonicated			Post Sonicated		
	UO_3	U_3O_8	UO_2	UO_3	U_3O_8	UO_2	UO_3	U_3O_8	UO_2
Specific surface area (m^2/g)	1.06	0.831	0.299	1.63	1.63	1.18	1.47	1.43	1.04
	1.39 (1)	1.55 (1)	0.73 (1)						
particle size (µm):									
10 percentile	3.54	4.01	49.7	1.37	1.62	1.85	1.92	2.19	2.51
50 percentile	9.16	14.0	111	8.02	11.2	53.2	7.72	9.24	32.5
90 percentile	21.1	31.0	178	24.5	32.1	150.3	23.2	26.1	141.2

(1) BET measurements

X-Ray diffraction spectra showed in Figure 6 demonstrate that UO_3 is partially hydrated, and confirms the oxidation state of UO_2, UO_3, and U_3O_8. Spectral analysis shows that approximately half the UO_3 is hydrated as $UO_3 \cdot 0.8H_2O$. The exact amount of the hydrate was determined by weight difference after drying the powder for 36 hours at 300°C. It was determined that 49.6% of the UO_3 is hydrated. This value was confirmed by determining UO_3 molecular weight using the U concentration in the powders, obtained by ICP-OES after dissolution in nitric acid. Results from the ICP-OES are shown in Table 3; more detailed results are shown in Appendix A.

Table 3. Oxides molecular weights determined by ICP-OES

Oxide	UO_2	U_3O_8	UO_3
[U oxide] prepared (ppm)	408	432	654
[U] by ICP-OES (ppm)	360	371	533
MW theoretical ($mol.g^{-1}$)	270	842	286
MW by ICP-OES ($mol.g^{-1}$)	269	826	292
Bias on MW (%)	0.55%	1.9%	--

% hydrate (0.8 H_2O) in UO_3	--	--	43%

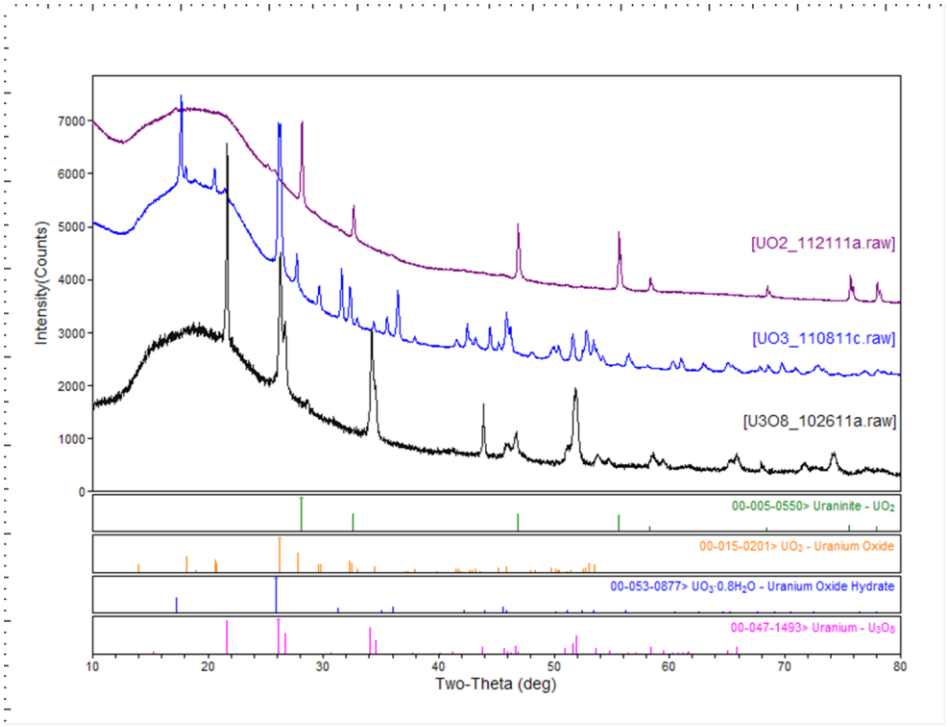

Figure 6. X-Ray Diffraction spectra of uranium oxide powders (UO_2, UO_3, and U_3O_8)

4. ONLINE MONITORING IN SC-CO_2 WITH UV-VIS SPECTROSCOPY

4.1 Schematic and pictures of the extraction chamber with UV-Vis capability

A schematic of the extraction system is shown in Figure 7. Pictures of our actual system are shown in Figure 8 and Figure 9. It consists of a syringe pump (ISCO, model 500D) that pressurizes, regulates and delivers CO_2 to the system. The entire setup is rated up to 5000 PSI. The total volume of the system was measured to be 34.8 ± 0.5 mL with R1 in line and 25.3 ± 0.3 mL without R1. The reactor cell (R1) is a 7.5 mL column with an entry and an exit for the fluid at each end. The extractant (TBP complex) is delivered to this cell at the start of an experiment via a syringe. The high-pressure extraction cell (R2) is where the uranium oxides are delivered prior to extraction. R2 fits inside an aluminum hot block which is temperature controlled by a thermocouple. R2 also doubles as a UV-Vis cell (S.I. Photonics, Tucson, Az), where fiber optics are used to measure the absorbance of the fluid and its components under pressure. The cell path-length between the fiber optics was measured to be 0.7 cm. The cell can also be stirred using a traditional magnetic stirrer inside the cell that is controlled by the stirring plate on which the hot block sits.

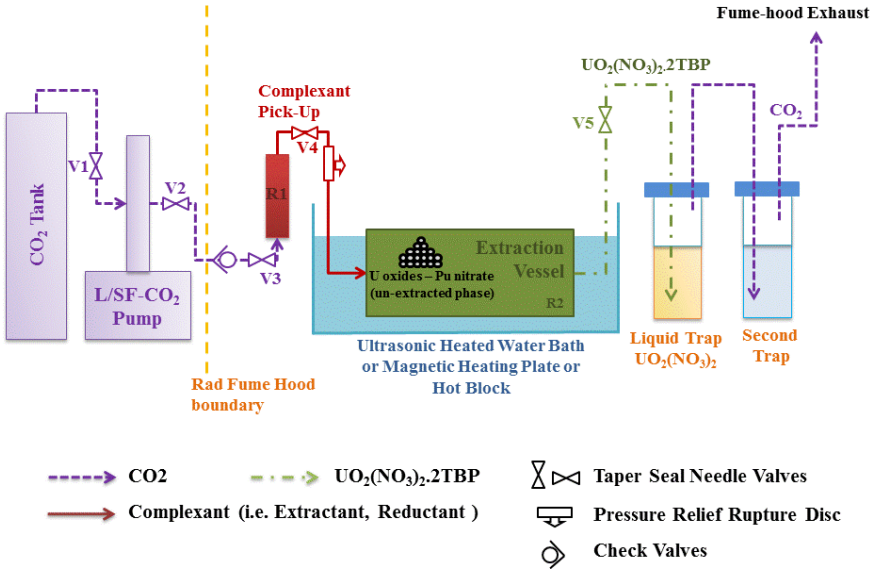

Figure 7. Schematic of the SFE system in use at PNNL

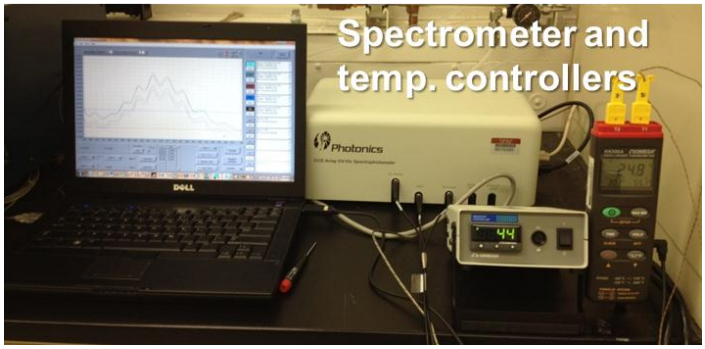

Figure 8. Spectrometer, process monitor and temperature controllers

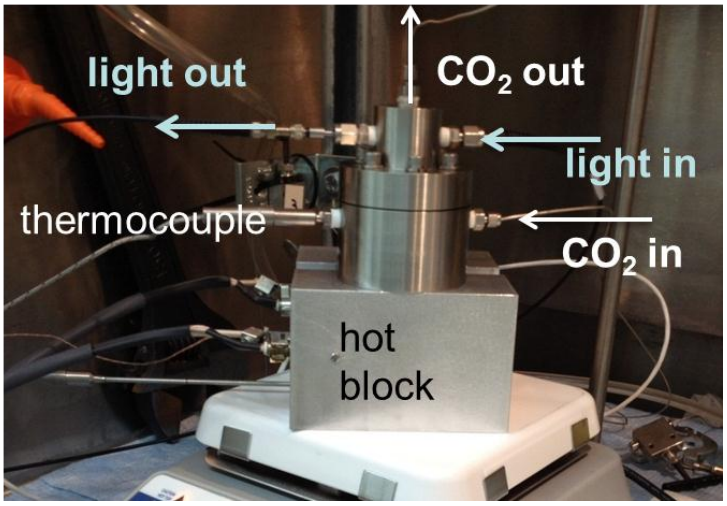

Figure 9. Extraction cell (R2, on top of the hot block for better view) with online monitoring

4.2 Spectrum analysis

In the literature, uranium absorbance is generally taken at 414 nm and its value is corrected with a reference at 375 nm, as seen on Figure 10. This traditional method works well when the TBP/HNO_3 concentration in CO_2 is low and relatively constant. Indeed, with this configuration, the tailing from the TBP/HNO_3 peak (0 mg U trace in Figure 10) has a small influence on uranium absorbance and is relatively consistent from one setting to the other.

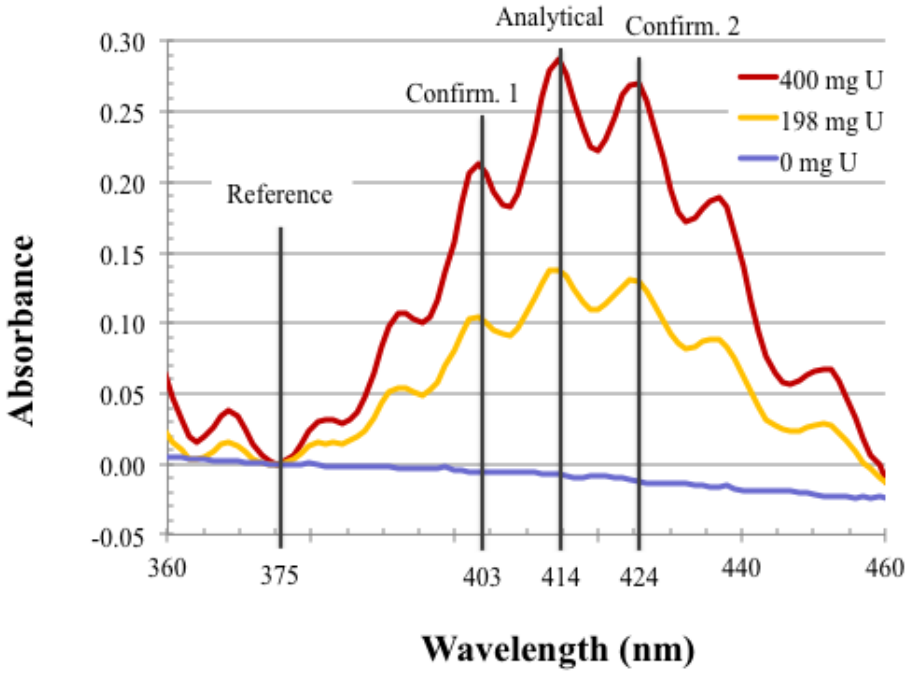

Figure 10. UV-Vis spectra of U(VI) extracted with TBP at different uranium concentrations in supercritical CO_2 at 50°C and 2900 PSI.

However, when the TBP/HNO_3 concentration is higher or changes from one experiment to the other, the contribution of the TBP/HNO_3 peak to the uranium peak can be greater and inconsistent, as seen on Figure 11. In the second spectrum (3rd trace) in Figure 11 the uranium absorbance would be negative with the traditional method, although there is obviously some uranium in the system. We decided therefore to use a deconvolution method to approximate the TBP/HNO_3 peak and its contribution to the uranium absorbance. We used a Gaussian function (Equation 1) for the deconvolution because this function is known to fit UV-Vis absorbance peaks the best.[9] We used a least squared method to find the best fitting function for each TBP/HNO_3 peak.

$$A = A_{max} e^{-4ln2\frac{(\nu-\nu_{max})^2}{\Delta\nu^2}} \qquad \text{Equation 1}$$

Where A is the Absorbance at wavenumber ν (in cm^{-1}, $\nu=10^7/\lambda$ with λ the wavelength in nm), A_{max} is the absorbance maximum at wavenumber ν_{max}, and Δν is the half band width.

This method has been proven reliable, as it has been tested with standards at varying TBP/HNO_3 ratios and uranium concentrations in CO_2. We use this method for this work to calibrate our system and determine extraction efficiencies and uranium solubility at various pressure and temperature in CO_2. Furthermore, this method could be easily used in the future for the online monitoring of an sc-CO_2 separation plan.

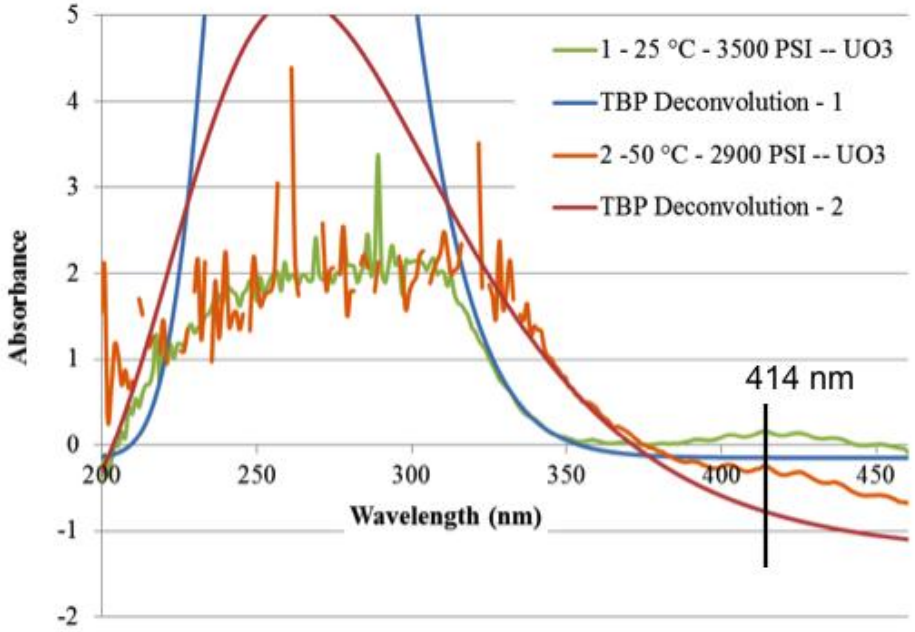

Figure 11. UV-Vis Spectra of U(VI) in the presence of TBP/HNO_3 in supercritical CO_2. Demonstration of the deconvolution method for two different TBP/HNO_3 peak contributions.

4.3 Calibration data

To calibrate the spectrometer, we dissolved a known amount of UO_3, UO_2 and U_3O_8 in $TBP(HNO_3)_{1.8}(H2O)_{0.4}$. A known volume (typically 2mL) of the resulting $UO_2(NO_3)_2$.2TBP complex dissolved in TBP-HNO3 is then introduced in the extraction cell (R2). The system is then pressurized at the lowest planned density setting and left for half an hour for dissolution and diffusion to occur in L/$ScCO_2$. Temperature and pressure are then modified for the next planned setting. For this operation and

to avoid any loss of analytes, we never decrease the density. Once the temperature is stable at its new setting, the system is left to equilibrate for 10 min before the next setting adjustment. Full UV-Vis spectra are taken every 2 minutes and recorded for later analysis as described in the previous section.

Figure 12 graphs show the absorbance values recorded for the uranium peak at 414 nm versus the uranium concentration at various pressure and temperature settings. More graphs are shown in Appendix B, C and D. The plots are linear, and the slopes provide the molar extinction coefficients (ε, also called molar absorption coefficient, or molar absorptivity) for each temperature and pressure settings according to the Beer-Lambert law stated in Equation 2.

$$A = -\log_{10}\frac{I}{I_0} = \varepsilon l c \qquad \text{Equation 2}$$

Where A is the Absorbance, I and I_0 are the light intensities of the transmitted light and the incident light, respectively, l is the light pathlength (cm), c the concentration ($mol.L^{-1}$) and ε the molar extinction coefficient ($L.mol^{-1}.cm^{-1}$).

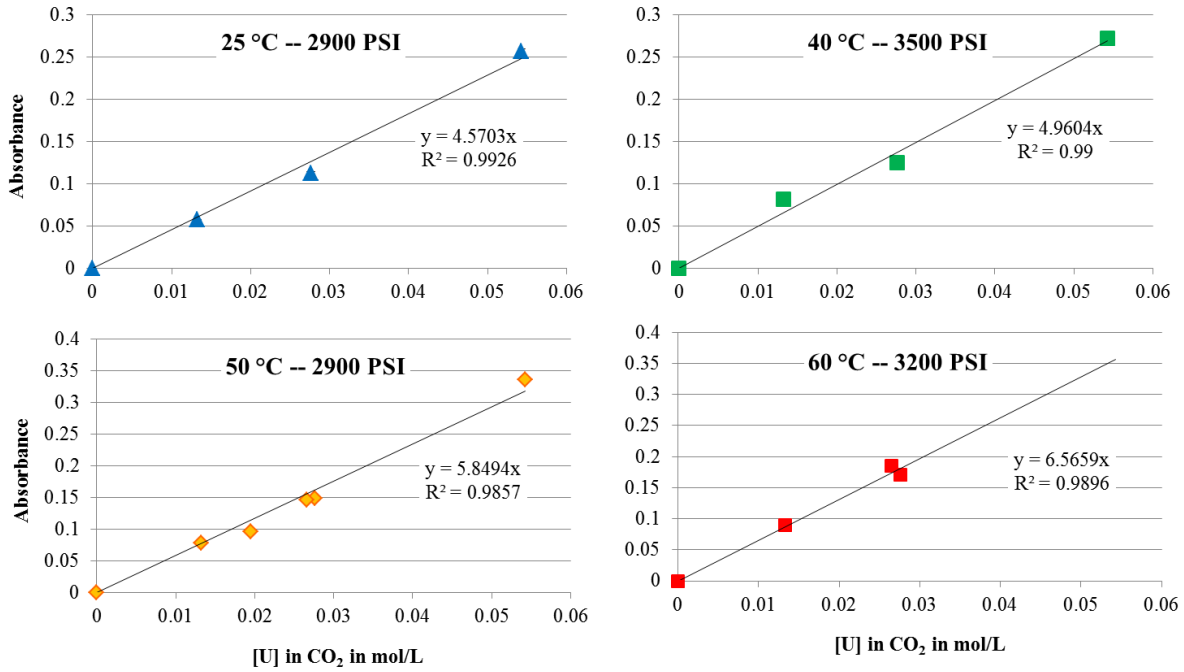

Figure 12. Absorbance vs. uranium concentration (mol/L) in l/sc-CO_2 for the molar extinction coefficient determination at 414 nm for different temperature and pressure settings

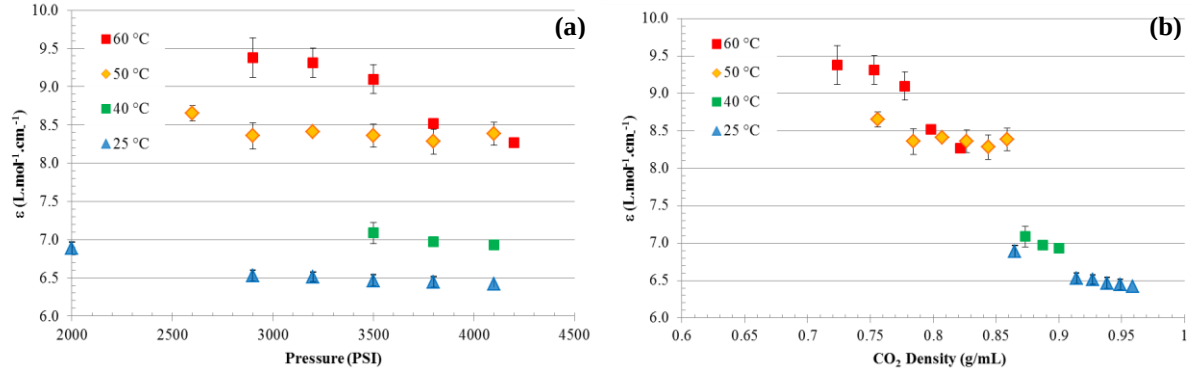

Figure 13. Molar extinction coefficients (mol.L^{-1}.cm^{-1}) for varying pressures (a) and densities (b) between 25 and 60 C.

Figure 13a shows the influence of the pressure for different temperature settings on the extinction coefficient for the uranium peak at 414 nm. The same values are plotted versus the density in Figure 13b. As the temperature drops, the extinction coefficient decreases. It also decreases slightly with increased pressure. The decrease is stronger when the density increases.

Once the coefficients have been determined, the Beer-Lambert law can be used to determine the unknown concentration of uranium following dissolution in the l/sc-CO_2.

5. $UO_2(NO_3)_2(TBP)_2$ DISSOLUTION

In this section, the results from $UO_2(NO_3)_2(TBP)_2$ solubility tests in CO_2 and the influence of the temperature and the pressure on the solubility are discussed.

The $UO_2(NO_3)_2(TBP)_2$ complex was made by dissolving 1g of UO_3 in TBP-HNO_3. The whole amount was introduced in the extraction cell (R2) and UV-Vis spectra were recorded every 2 min. The uranium concentration ([U] in mol/L) in the CO_2 phase was determined by analyzing these spectra with the methodology described above. Figure 14 shows [U] for different pressure and temperature settings. Each data point is calculated from an average of 2 to 5 spectra taken after the dissolution equilibrium was reached. At 40°C, [U] reaches a plateau as, all the $UO_2(NO_3)_2(TBP)_2$ is dissolved in the CO_2 phase. The 50°C and 2900 PSI setting offers the best compromise, as more than 90 % of the complex is dissolved while keeping the pressure at a reasonable level. At 25°C, where CO_2 is liquid, not supercritical, the solubility is lower and varies little with increasing pressure. At 60°C, the added benefit of the higher temperature is overcome by the loss in density, and therefore the pressure needs to go to ~4000 PSI to reach the solubility measured at 40 and 50 °C.

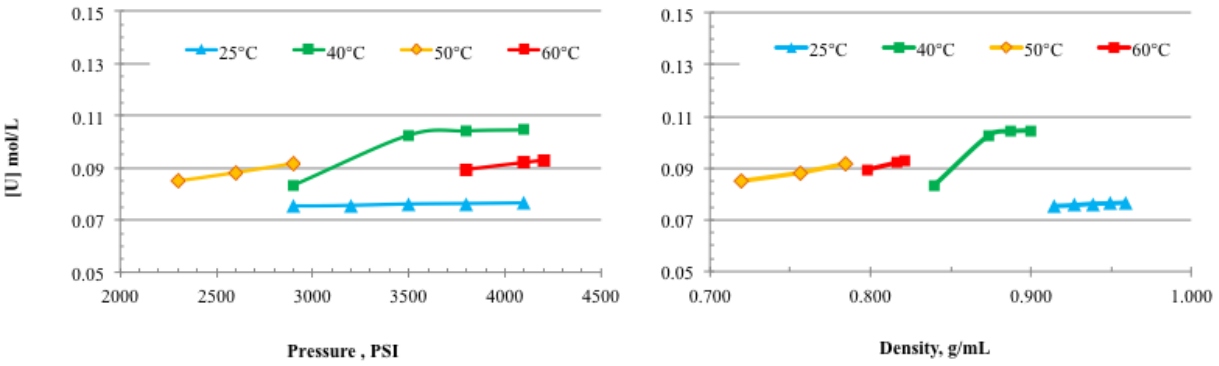

Figure 14. Uranium concentration in CO_2 measured by UV-Vis at different temperature settings vs. pressure (a) and density (b).

6. DISSOLUTION OF URANIUM OXIDES

6.1 Influence of CO_2 temperature, pressure, and density on extraction

If the fluid density is kept above 0.8 g/mL, the temperature and pressure does not influence the dissolution in a measurable manner. More experiments are planned with increased amounts of uranium oxides (we typically use 500 mg per run) to push our system to the point where accountable differences may be observed.

6.2 Influence of the TBP complex used on extraction

For this process, uranium is not dissolved in nitric acid. However, nitric acid is still required to oxidize uranium oxides to U(VI) and make it available for extraction. In order to introduce nitric acid in the system, we make TBP/HNO_3 complexes by contacting concentrated nitric acid with TBP and by extracting the resulting organic phase.

6.2.1 TBP complex formation and characteristics

Different TBP/HNO_3 complexes can be made by simply modifying the volume ratios between the organic phase (TBP) and the aqueous phase (HNO_3 at 15.8 M). The contact time between the two phases is typically 10 minutes of vigorous shaking, and is followed by centrifugation for 30 minutes at 3000 rpm. Table 4 shows the different ratios between TBP, nitric acid and water in the complexes made using this method. The highlighted complexes in this table were used to assess the influence of the TBP complex on the uranium extraction efficiency.

Table 4. TBP/Nitric acid complex characteristics for different initial HNO_3/TBP volume ratios.[3]

	Initial volume (mL)		Molecular ratio in the org. phase		
Ratio aq. phase / org. phase	Aq. phase (HNO_3)	Org. phase (TBP)	HNO_3/ TBP	H_2O / TBP	HNO_3/H_2O
0.00	0	5	0	1.06	0.00
0.10	0.5	5	0.42	0.83	0.51

0.10	1	10	0.42	0.74	0.57
0.17	1	6	0.71	0.73	0.97
0.20	1	5	0.81	0.42	1.93
0.22	1	4.5	0.88	0.46	1.91
0.25	1	4	0.97	0.41	2.37
0.33	1	3	1.13	0.36	3.14
0.50	1	2	1.38	0.4	3.45
1.00	1	1	1.8	0.44	4.09
2.00	2	1	2.13	0.54	3.94
3.00	3	1	2.29	0.48	4.77
6.00	6	1	2.37	0.53	4.47

As the ratio between the aqueous (aq.) and the organic (org.) phase increases, more nitric acid is dissolved in the organic phase. Concurrently, the amount of water relative to the amount of nitric acid decreases. This should benefit the extraction, as more nitric acid is available to oxidize the uranium. However, the increase of the nitric acid to water and to TBP ratios in the organic phase tapers off after a 1:1 initial volume ratio between the organic and the aqueous phase is reached. It would therefore be unproductive and wasteful to use higher initial aqueous to organic phase ratios.

6.2.2 Dissolution and extraction results

To assess the complex composition influence on the extraction, we prepared the different complexes highlighted in Table 4. Figure 15 shows the percent of UO_3 extracted in CO_2 at 2900 PSI and 50°C using these complexes. The extraction efficiency decreases as the nitric acid to water ratio in the complex decreases. This shows that maintaining a high nitric acid to water ratio in the organic phase is essential for the best extraction results.

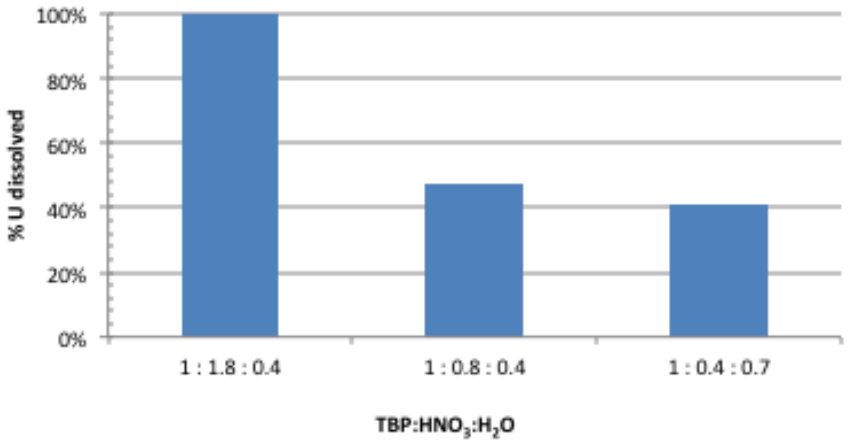

Figure 15. % uranium dissolved in sc-CO2 (2900 PSI, 50°C) using different TBP/nitric acid complexes

6.3 Influence of the type of oxide used on extraction

The UO_2 and UO_3 have different dissolution mechanisms in TBP containing nitric acid as described in Equation 3 and 4 below. UO_2 dissolution byproducts are water and nitric or nitrous oxide while UO_3 produces only water. U_3O_8 as a 1:2 mixture of UO_2 and UO_3 combine both mechanisms (Equation 5).

$$UO_2 + \frac{8}{3}HNO_3 + 2TBP \rightarrow UO_2(NO_3)_2.2TBP + \frac{4}{3}H_2O + \frac{2}{3}NO$$

Equations 3

$$\text{or } UO_2 + 4HNO_3 + 2TBP \rightarrow UO_2(NO_3)_2.2TBP + 2H_2O + 2NO_2$$

$$UO_3 + 2HNO_3 + 2TBP \rightarrow UO_2(NO_3)_2.2TBP + H_2O$$

Equation 4

$$U_3O_8 + \frac{20}{3}HNO_3 + 6TBP \rightarrow 3UO_2(NO_3)_2.2TBP + \frac{10}{3}H_2O + \frac{2}{3}NO$$

Equations 5

$$\text{or } U_3O_8 + 8HNO_3 + 6TBP \rightarrow 3UO_2(NO_3)_2.2TBP + 4H_2O + 2NO_2$$

These equations suggest that UO_3 would be extracted more efficiently than UO_2. Also, U_3O_8 extraction efficiency would be between UO_3 and UO_2. However, experimental results showed on Figure 16 indicate a slightly better dissolution rate for UO_3 over UO_2, while showing only 35% extraction efficiency for U_3O_8.

We are still investigating the reason behind this behavior. Particle size is not an issue, since it was measured and U_3O_8 particle size was found to be similar to UO_3 and smaller than UO_2. This might be caused by the crystal structure of U_3O_8. We are also looking into acquiring U_3O_8 from another supplier, or into making some U_3O_8 from the UO_2 available, in order to understand if the results are specific to the oxide used or if they can be generalized to other U_3O_8 preparations.

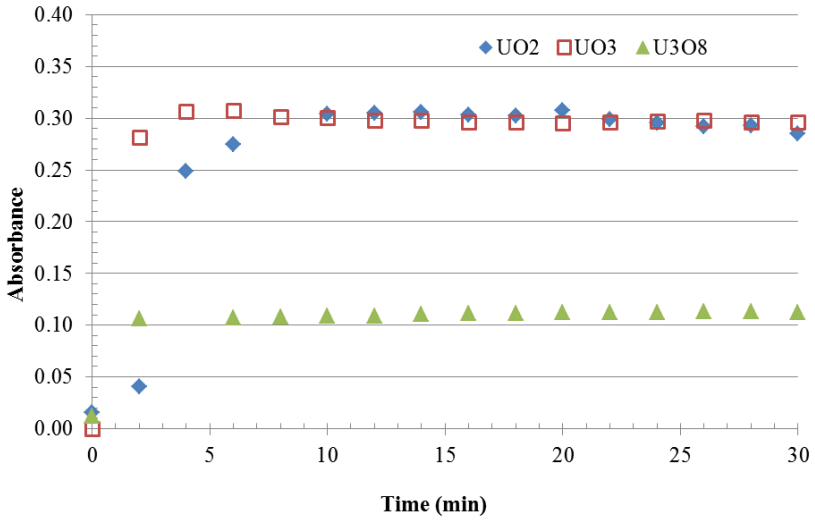

Figure 16. Dissolution of 0.3 g of different uranium oxide in sc-CO2 at 50°C and 2900PSI using 2mL of $TBP(HNO_3)_{1.8}(H_2O)_{0.4}$

7. URANIUM BACK EXTRACTION INTO AN AQUEOUS PHASE

We are evaluating methodologies for the back-extraction of the organically complexed uranium from the organic phase into an aqueous phase. In an ideal reprocessing scenario, the sc-CO_2 carries the $UO_2(NO_3)_2$.2TBP complex away from the fuel meat. The sc-CO_2 enables efficient transport of the uranium to an engineered plant component (e.g., counter-current columns, mixer-settlers, or centrifugal contactors) capable of enabling the phase transfer of uranium from the organic to an aqueous phase (after which uranium is converted to a solid oxide). In the case of sc-CO_2 utilization, the back-extraction process requires that the aqueous phase be at similar temperature and pressure as the sc-CO_2.

7.1 Off-line liquid liquid extraction methods

In the interim, we initially evaluated (off-line) liquid-liquid extraction methods for efficient removal of complexed uranium ($UO_2(NO_3)_2$.2TBP) into an aqueous phase. We chose to evaluate carbonate and sulfate solutions, as they are well known agents for uranium back-extraction.[10,11] Utilization of the ammonium counter-ion has additional benefits, as it can be added or removed as a gaseous component (as NH_3). Furthermore, the use of carbonate is also potentially beneficial, as it also can be added or removed as a gaseous component (as CO_2).

According to Equation 1, ammonium carbonate can be created in a high-pressure environment with the addition of anhydrous NH_3 to CO_2 in the presence of water:

$$CO_2 + 2NH_3 + H_2O \rightleftharpoons (NH_4)_2CO_3 \qquad \text{Equation 6}$$

This approach represents a potentially recyclable reagent system whereby the gaseous reagents can be used to tune the ammonium carbonate concentration in the aqueous phase and therefore maximize uranium recovery.

Figure 17 shows the uranium recovery from the TBP phase (◊) and into a 1M $(NH_4)_2CO_3$ aqueous solution over increasing aqueous to organic phase volume ratios. This figure also shows the final pH of the aqueous phase following the back extraction (□). We observed that uranium recoveries in the aqueous phase are typically >90% once the pH of the ammonium carbonate solution reaches ≥6.5. Similar results were obtained while using other salts in the aqueous phase such as sodium carbonate and sodium bicarbonate.

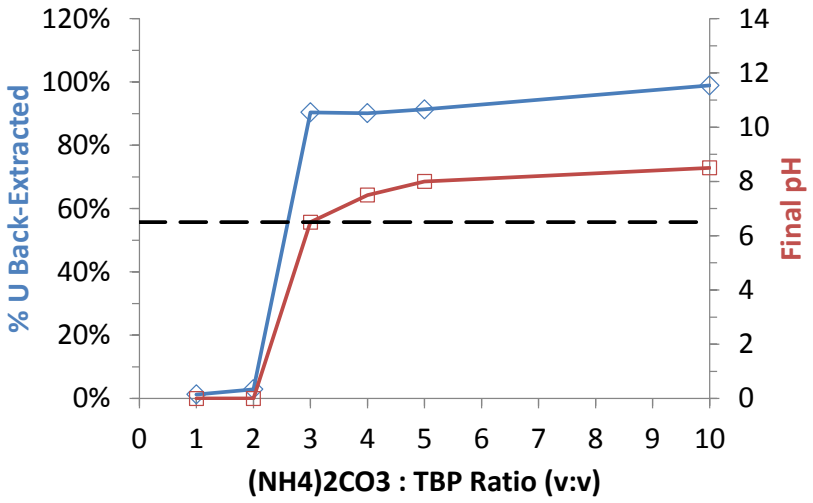

Figure 17: Recovery of uranium from $UO_2(NO_3)_2.2TBP$ (◊) and final aqueous phase pH (□) at various aqueous to organic volume phase ratios using a 1M $(NH_4)_2CO_3$ aqueous phase solution.

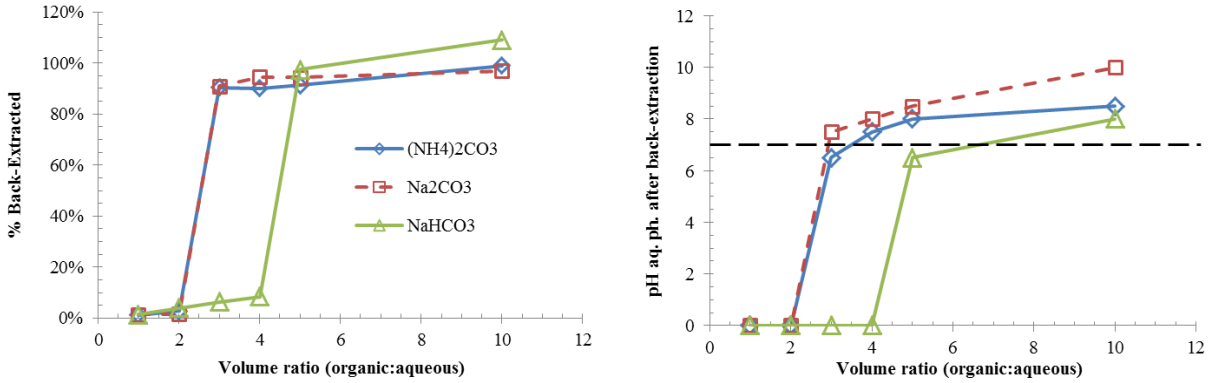

Figure 18. Recovery of uranium from $UO_2(NO_3)_2.2TBP$ and final aqueous phase pH at various aqueous to organic volume phase ratios using different carbonate salts in the aqueous phase.

These sets of data were performed at relatively low uranium concentrations (~12 µg/mL U in the TBP). This concentration needed to be scaled up in order to more closely match the actual organic phase formed during the SFE process. Therefore, we explored uranium recoveries for significantly higher initial uranium concentrations in the organic phase.

Based on the data from Figure 17, we decided to use a 6:1 aqueous to organic phase ratio with an aqueous solution at 2M $(NH_4)_2CO_3$ to ensure nearly quantitative recovery of uranium. Figure 19 shows the resulting three-phase solutions (top to bottom: TBP, aqueous, and solid phases) with decreasing initial uranium concentration in the organic phase from left to right (ranging from 0.19 g/mL down to 0.007 g/mL). Table 5 summarizes the initial uranium concentration and the final uranium distribution in each of the three phases. For all concentrations, recoveries of uranium in the aqueous phase are above 90%. However, as the initial uranium concentration increases in the organic phase, the amount of precipitate desalting out of the aqueous phase likewise increases.

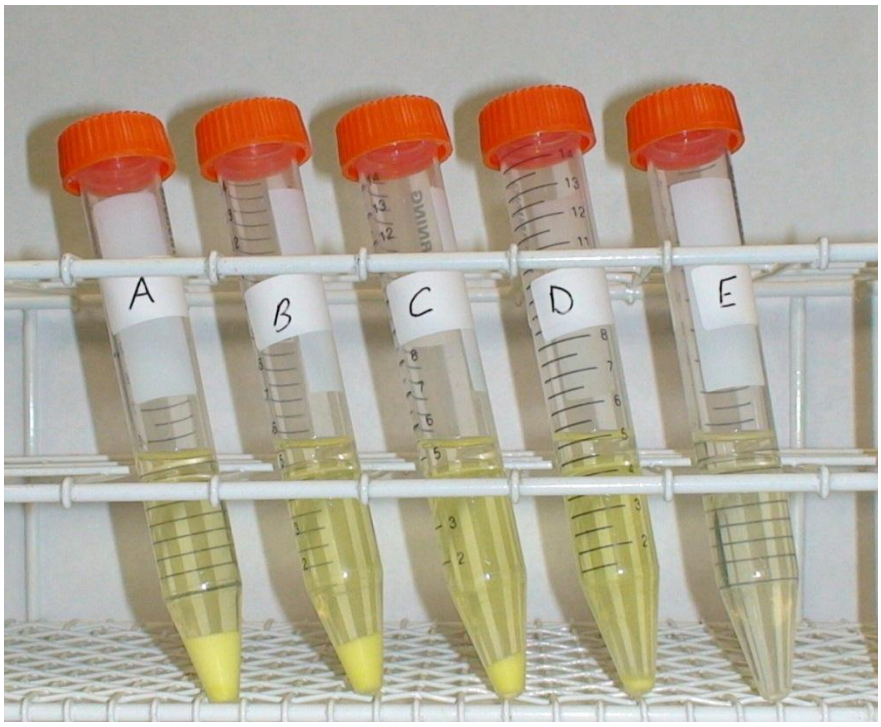

Figure 19. Picture of all phases (organic on top) after uranium back extraction. Aqueous to organic volume phase ratio was 6:1. Aqueous solution made of 2M $(NH_4)_2CO_3$. The initial uranium concentration decreases from left to right, see Table 5.

Table 5. Recovery of uranium from the organic phase via back extraction in 2M $(NH_4)_2CO_3$. Aqueous to organic volume phase ratio was 6:1, see Figure 19.

Label	A	B	C	D	E
[U] initial (mg/mL)	190	130	70	40	7
% U in organic phase	0.0	0.0	0.0	0.0	0.2
% U in aqueous phase	**94.5**	**93.6**	**92.5**	**93.1**	**98.9**
% U in precipitate (inferred)	5.5	6.4	7.5	6.9	0.9

We analyzed, via radiometric counting, the TBP and the aqueous phases to determine the distribution of uranium. We infer that any missing activity of uranium is therefore in the solid phase. However, the precipitate contains only a small portion of uranium, between 0 and 8% of the total mass and does not interfere with the back extraction efficiencies. This chemistry, however could not be used in an "in-line" setting where precipitates could potentially block the flow of the sc-CO_2 in the system.

Hydrogen peroxides react with carbonates to form peroxymonocarbonate ions and with uranyl carbonate to form the uranyl peroxo-carbonato complex.[12] The products formed with these reactions are more soluble in the aqueous phase. Thus, we tested hydrogen peroxide as a complexing agent to increase salt solubility in the aqueous phase and avoid the formation of a precipitate. Figure 20 shows the action of different concentrations of hydrogen peroxide on the precipitate formation and on the phase distribution

of uranium. At a concentration of 0.1M H_2O_2 and above, no precipitate was observed. Additionally, there is no quantifiable effect on the addition of hydrogen peroxide uranium phase partition. We reanalyzed both phases (Figure 20), and no uranium was detected in the organic phase.

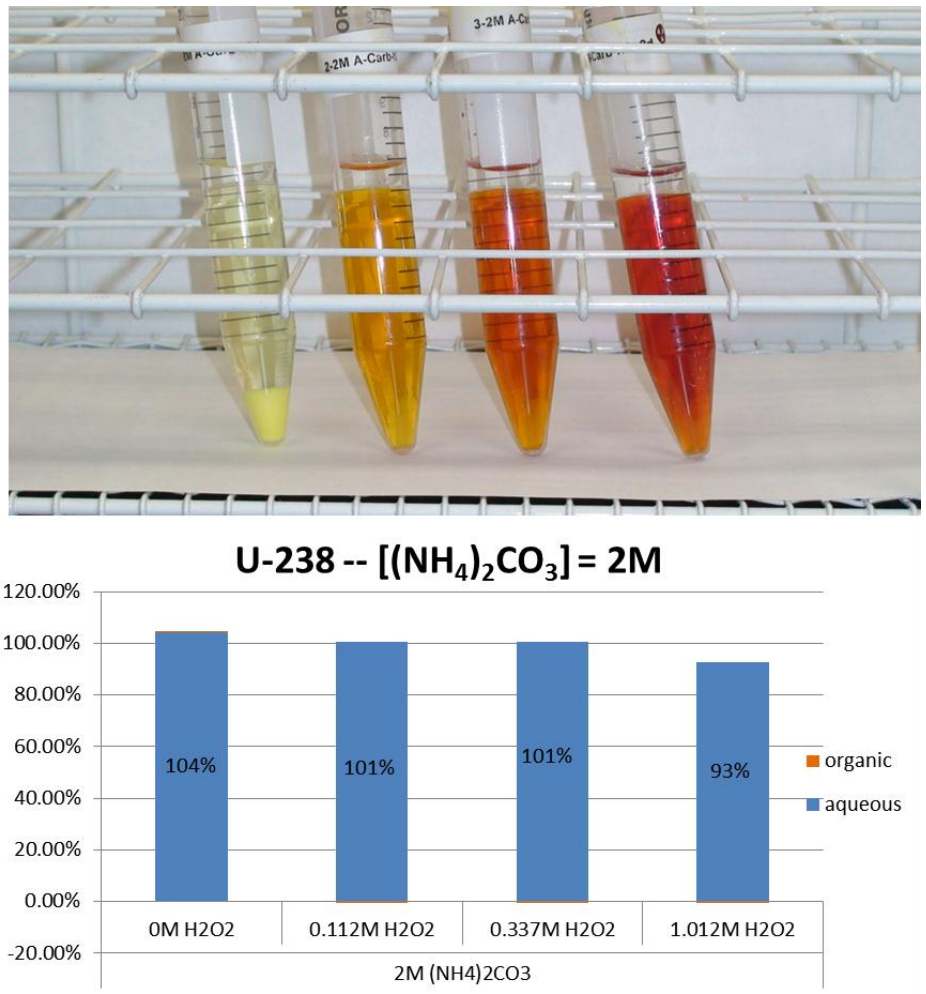

Figure 20. Effect on the addition of H_2O_2 (0 to 1 mol/L) on the precipitate formation for the conditions A in Figure 19 and Table 5 i.e., [U]=192 mg/mL, [(NH4)2CO3]=2 mol/L

7.2 In-line back extraction using a stripping column

A prototype for a stripping column was engineered to back extract uranium into an ammonium carbonate and hydrogen peroxide solution. The schematic and picture of the column are shown on Figure 21. The system allows for the pressurization of the stripping column with CO_2 before the start of the back extraction. After the cell is pressurized to 1500 PSI with CO_2, the extracted phase (i.e., CO_2 phase containing the extracted $UO_2(NO_3)\cdot 2TBP$ complex) bubble into an ammonium carbonate (2 mol/L) and hydrogen peroxide (0.337 mol/L) solution. The bubbling action should strip the uranium from the organic phase and the TBP loaded CO2 can them be recovered in a complexant trap.

Unfortunately, initial experiments were not successful. Under various conditions, part of the ammonium carbonate solution back flowed out of the stripping column and into the complexant trap. The use of a larger column, which would contain the stripping solution better is a possible solution to this problem. Adjustment of the ammonium carbonate solution volume, the back extraction flow rate and the CO_2 initial pressure in the column can also remediate this problem. However, within the timeline of this project, we were unable to fine tune the in-line back extraction process. Additional time and resources are required to engineer and test a suitable in-line back extraction process.

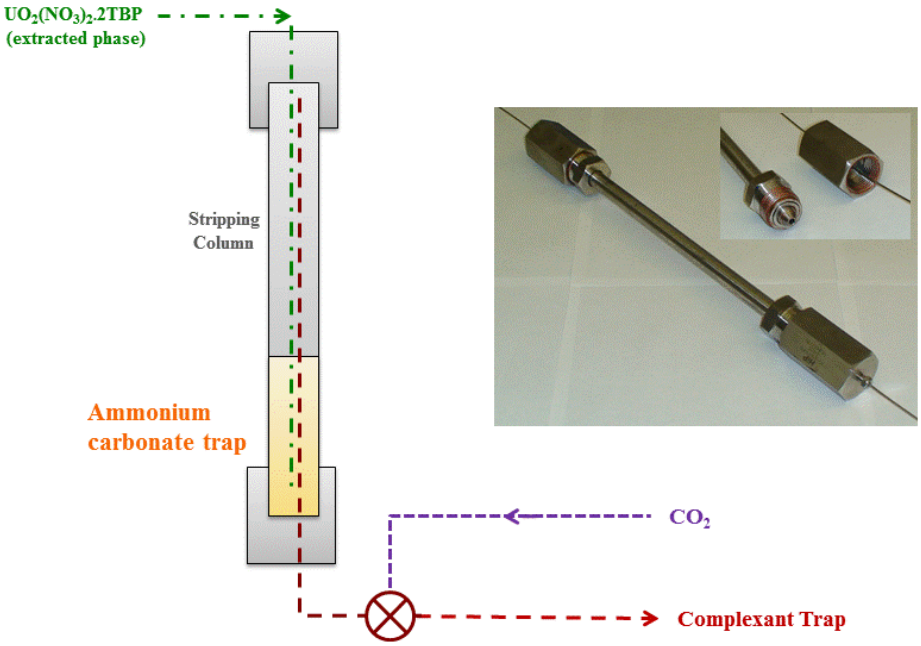

Figure 21. Prototype stripping column design used for back extraction. The whole system is shown in Figure 1.

However, despite not having a fully engineered system design, we were still able to show the feasibility of the back extraction with uranium oxides dissolved into sc-CO_2 using our SFE system. To demonstrate this, we dissolved the $UO_2(NO_3)_2.2TBP$ complex in CO_2 and let it bubble into a trapping solution of 2M $(NH_4)_2CO_3$ with different concentrations of hydrogen peroxide, as shown in Figure 22. Hydrogen peroxide disproportionate faster under the bubbling action and its concentration is therefore reduced in the trapping solution. To counteract this effect, we used a syringe to re-inject hydrogen peroxide into the trapping solution every 30 min.

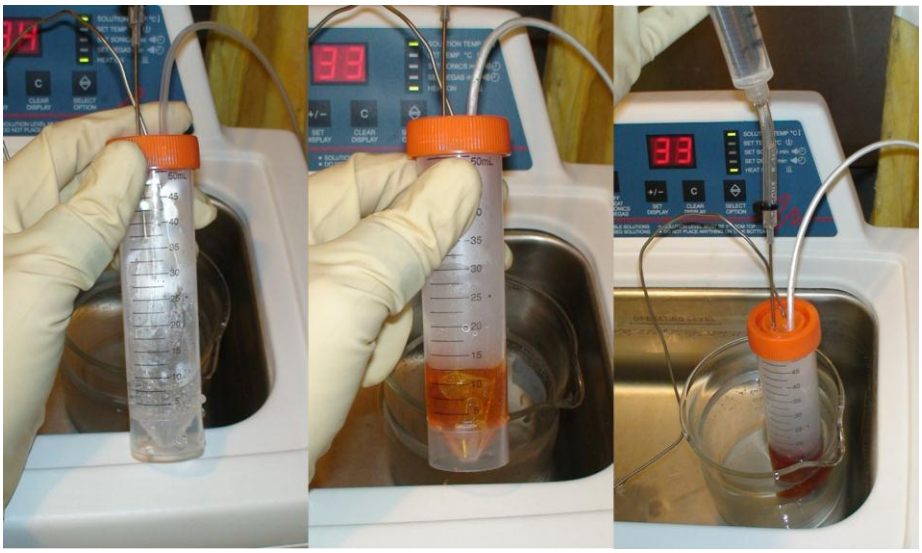

Figure 22. Ammonium carbonate trapping solution setup.

After two hours of back extraction with a CO_2 flow rate of 0.5 mL/min, we recovered both phases (the aqueous ammonium carbonate phase and the TBP organic phase) into the back extraction tube. Both phases were then analyzed for uranium concentration. Over 95% of the uranium was recovered into the aqueous phase. No uranium was detected in the organic phase. This demonstrated a successful uranium back extraction from the $UO_2(NO_3)_2$.2TBP loaded sc-CO_2 phase into $(NH_4)_2CO_3$ and H_2O_2.

7.3 Recovery of uranium from the stripping solutions to close the cycle

To close the cycle, we demonstrated the recovery of uranium from ammonium carbonate stripping solutions as purified uranium oxide. Stripping solutions containing different concentrations of hydrogen peroxide and ammonium carbonate (Table 6) were contacted with $UO_2(NO_3)_2$.2TBP complex in TBP. After the back extraction, the stripping solution were wet ashed in nitric acid (Figure 23 a.) to form $UO_2(NO_3)_2$ and then baked in an oven at 400C for 12 hours in air (Figure 23 b.) to form uranium oxide. XRD spectra of the residues were then obtained (Figure 24). The purified uranium was recovered as U_3O_8 powder under all conditions tested.

Table 6. Composition of the different stripping solutions used

ID / composition	1	2	3	4
$[(NH_4)_2CO_3]$ in mol/L	2.0	2.0	2.0	1.0
H_2O_2:U ratio	1:1	3:1	9:1	1:1

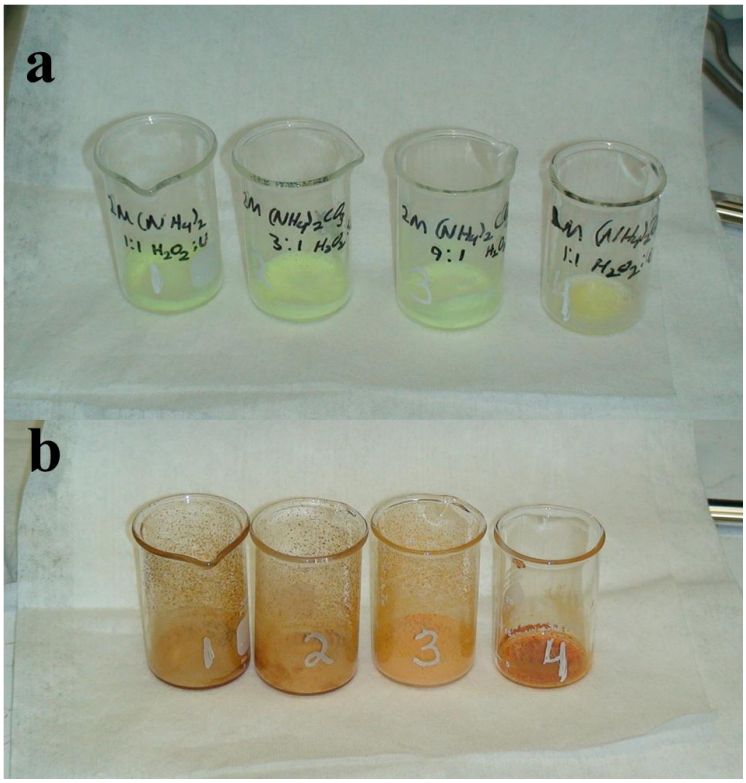

Figure 23. Uranium recovered from the stripping solutions after wet ashing (a) and baking at 400°C for 12 hours (b).

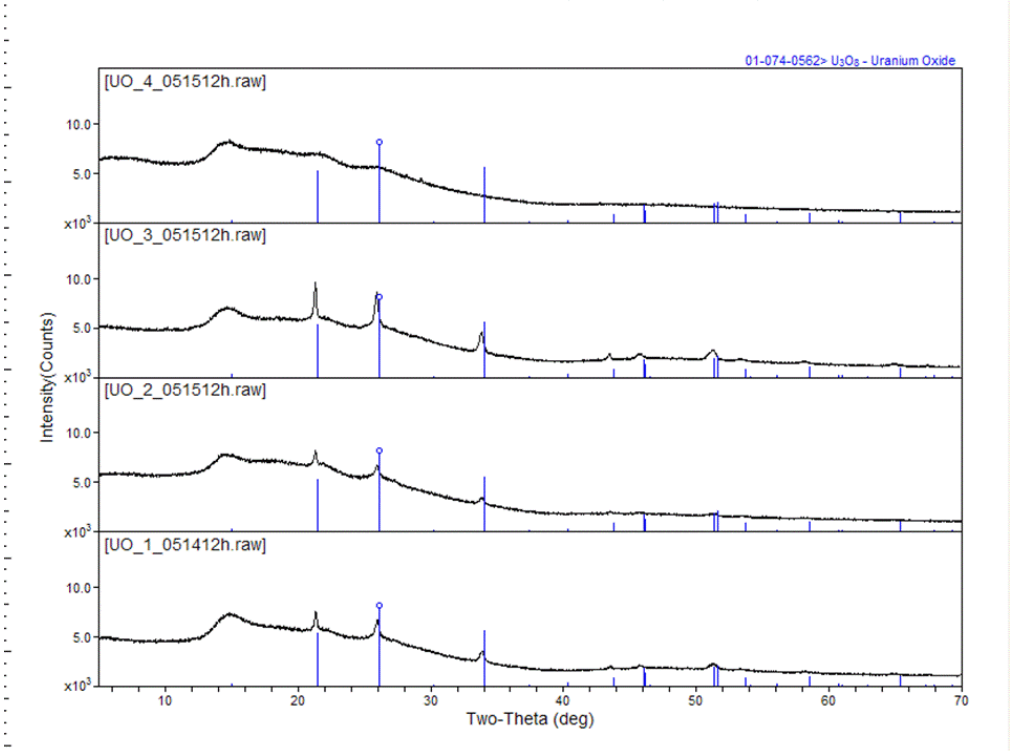

Figure 24. XRD spectra of the uranium complex after SFE, back extraction and recrystallization. Each sample indicates the presence of U_3O_8.

8. PLUTONIUM CO-EXTRACTION DETERENCE

Plutonium dioxide (PuO_2) can be extracted using the mechanism described above for uranium. Indeed, the nitric acid contained in the TBP/HNO_3 complex can oxidize PuO_2 to $PuO_2(NO_3)_2$ and extract it as $PuO_2(NO_3)_2 \cdot 2TBP$ complex. To limit the cost involved with using milligram quantities of plutonium oxide (glove box or hot cell containment), we started experimenting with plutonium nitrate (^{239}Pu) in dilute solutions (~60k dpm/mL, or ~0.44 µg/mL). The reasoning behind this is that plutonium nitrate should be more available for extraction than plutonium dioxide. Therefore, if we are able to inhibit the extraction of plutonium nitrate, we are most likely able to also inhibit the co-extraction of plutonium dioxide.

Plutonium exists predominantly in solution in three oxidation states: Pu (III), Pu(IV) and Pu(VI). Pu(IV) and Pu(VI) are extracted by TBP in sc-CO_2.[13] Considering the oxidizing media created by the HNO_3-TBP complex, Pu(IV) and Pu(VI) are preeminently present in our system. Therefore, a reductant or a complexant, or a combination of both, must be used to prevent plutonium co-extraction with uranium into the organic phase.

8.1 Use of AHA

8.1.1 Use of AHA with sc-CO_2 as the organic phase

To deter plutonium oxidation, the UREX process uses AHA (acetohydroxamic acid, $C_2H_5NO_2$) to reduce and complex plutonium, therefore inhibiting its extraction without affecting uranium extractability.[14] Our goal is to demonstrate this process in sc-CO_2.

Figure 25 shows NaI(Tl) scintillation spectra of the TBP-HNO_3 fraction after SFE of Pu-239 (left) or U-233 (right) spike at 50°C and 2900 PSI. The spike contained different amounts of nitric acid and/or AHA. Uranium (right) is not affected by the nitric acid concentration or by the addition of AHA. Plutonium extraction is slightly deterred when using AHA. The deterrence seems better at lower [AHA] (i.e., 0.1 mol/L vs. 0.3 mol/L). It is also better at lower nitric acid concentration (i.e., 1.4 mol/L vs. 2.4 mol/L). However, the amount of plutonium extracted was reduced by only 40% at the best test condition under pressure.

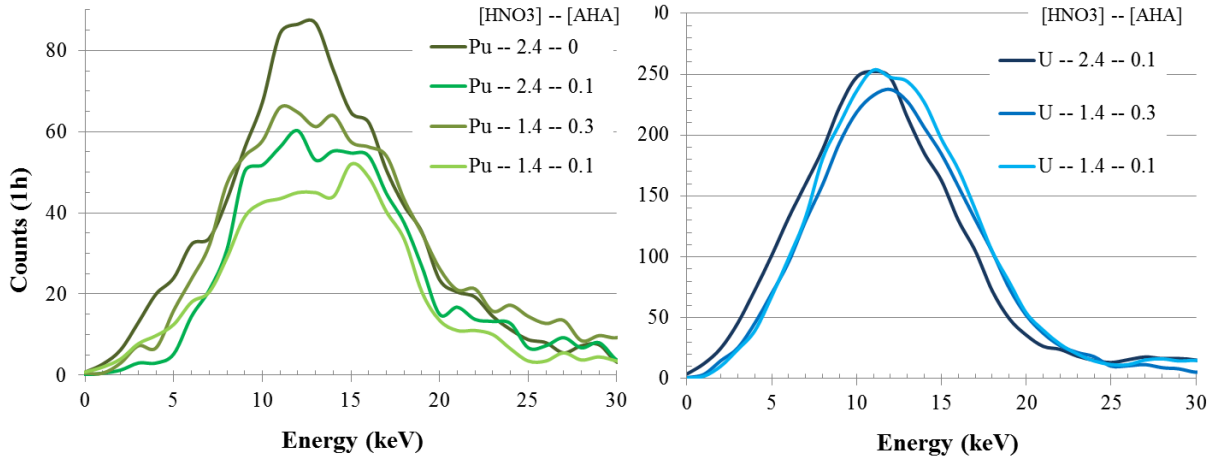

Figure 25. NaI(Tl) scintillation spectra of Pu-239 and U-233 from the TBP/HNO_3 fraction after SFE at 2900 PSI and 50 °C. Isotopes were introduced in the extraction cell with various [HNO_3] and [AHA] (mol/L).

8.1.2 Liquid-liquid extraction with dodecane as the organic phase

SFE experiments are time consuming. To find condition settings (i.e., AHA and nitric acid concentration, organic and aqueous phase volume ratio) that will disfavor plutonium co-extraction in a timely manner, we did batch contact experiments using a solution of 33% TBP in dodecane to simulate the sc-CO_2 phase. We contacted, for an hour, 0.25 mL of the aqueous phase containing a 3000 dpm spike and the reducing agent or complexant with 1 mL of the organic phase. The solutions were then centrifuged for 30 min and the two phases were separated. NaI(Tl) scintillation spectra were then taken for 0.75 mL of the organic phase, and 0.25 mL of the aqueous phase adjusted to 0.75mL with nitric acid at 1 M.

Figure 26 and Figure 27 show the partition of americium and uranium between the two phases. Uranium, and americium are not affected by the nitric acid or the AHA concentrations used in the aqueous phase. Indeed, their oxidation states are stable as U(VI) and Am(III). Therefore, uranium partitions into the sc-CO_2 phase while americium stays in the aqueous phase.

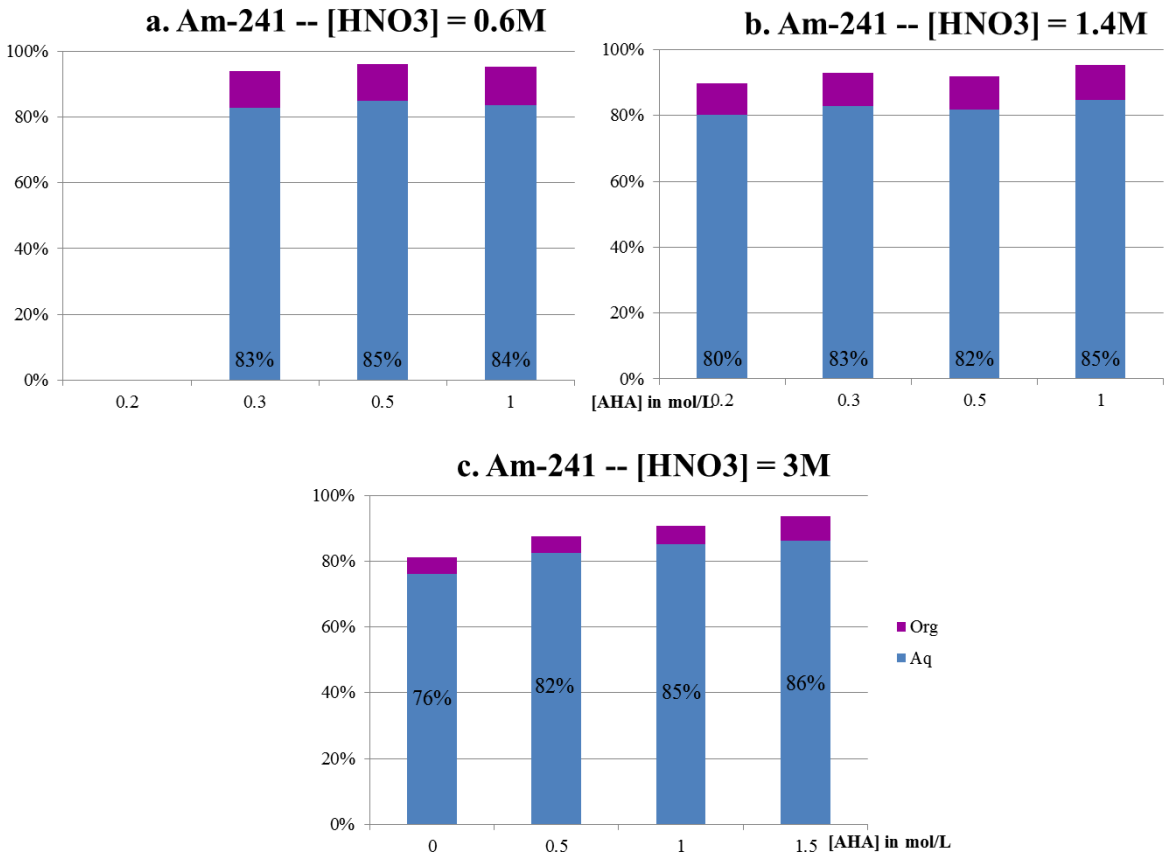

Figure 26. Americium partition between the organic and aqueous phase for different nitric acid and AHA concentrations in the aqueous phase.

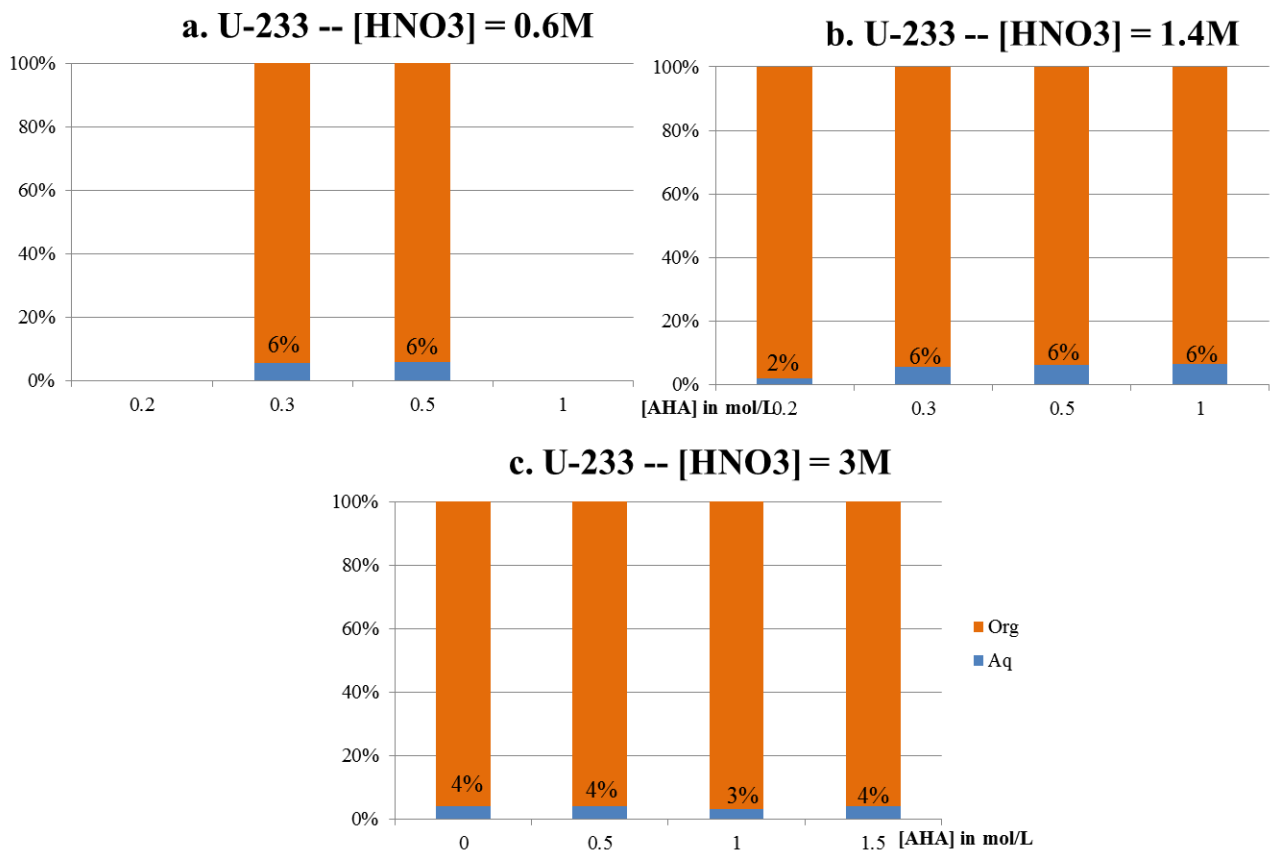

Figure 27. Uranium partition between the aqueous phase (measured) and the organic phase (inferred) for different nitric acid and AHA concentrations in the aqueous phase.

Plutonium however, can have different oxidation states under these conditions, i.e., Pu(III) if plutonium is reduced by AHA, Pu(IV) and possibly Pu(VI). Trivalent plutonium should behave as americium and stay in the aqueous phase. Tetravalent plutonium should be able to bind to AHA and stay in the aqueous phase while hexavalent plutonium should be extracted. Figure 28 shows batch contact results for plutonium under different nitric acid and AHA concentrations. Plutonium retention in the aqueous phase is improved at lower nitric acid concentration (i.e., 0.6M) and increases at higher AHA concentrations. The best plutonium retention (46%) was obtained in 0.6M HNO_3 and 1M AHA.

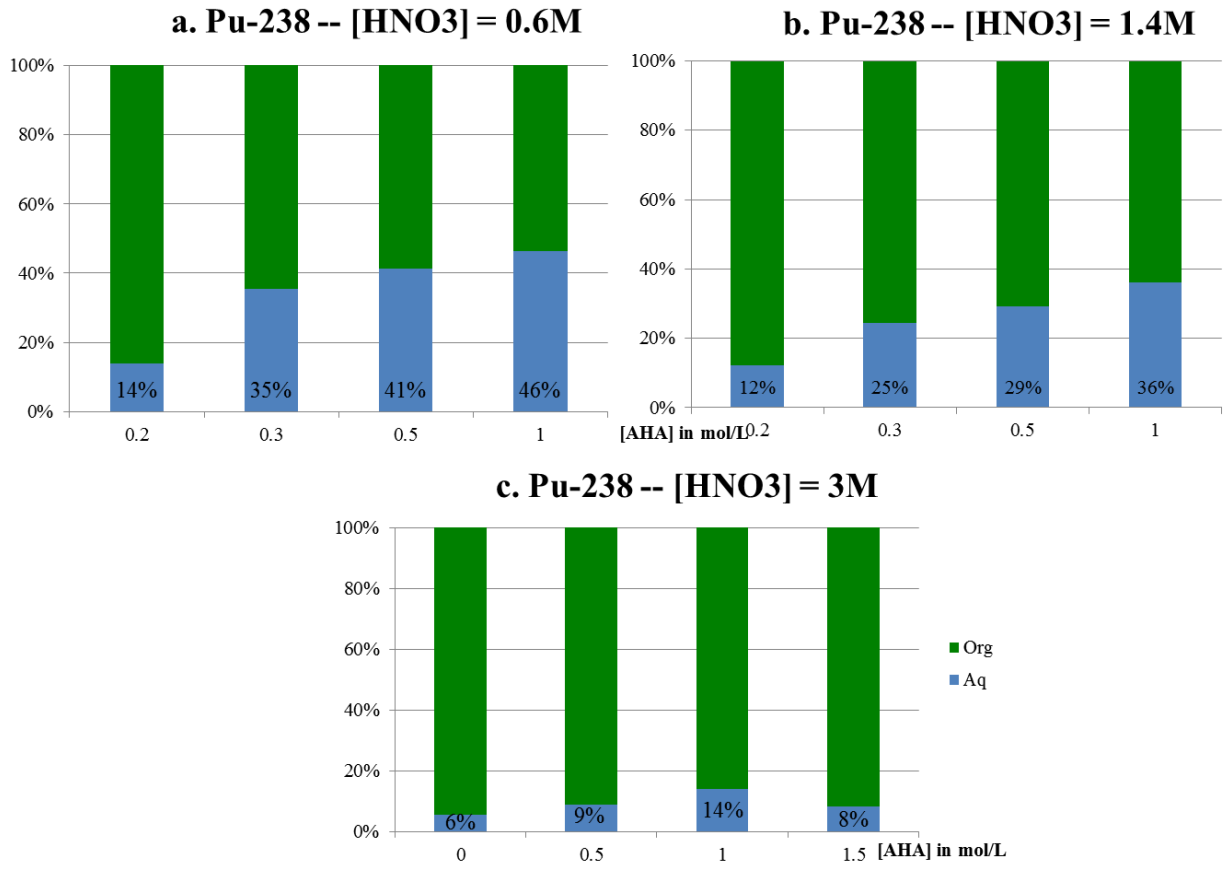

Figure 28. Plutonium partition between the aqueous phase (measured) and the organic phase (inferred) for different nitric acid and AHA concentrations in the aqueous phase.

8.2 Other Pu(IV) complexant or reductants

We were not able to reach high levels of separation using AHA as a complexant or reductant. Consequently, we investigated other possible reductants and complexants, and did additional batch contact studies, similar to those described in the previous section.

8.2.1 Fe(II) – ascorbic acid and hydroquinone

Ferrous ammonium sulfate ($FeSO_4(NH_4)_2SO_4 \cdot 6\ H_2O$) is often used by radiochemists to reduce Pu(IV) to Pu(III) in nitric acid. We hence tried this compound as a first alternative to AHA. We used ascorbic acid ($C_6H_8O_6$) as another reducing agent either alone to reduce plutonium or in combination with Fe(II), in order to maintain the iron in its divalent state. Hydroquinone ($C_6H_4(OH)_2$) was the third reducing agent explored. Figure 29a show that none of these reducing agents were able to affect Pu retention in the organic phase. Consequently, a complexant needs to be added to reach this goal.

AHA is often characterized as a complexant to Pu(IV), we therefore combined these reductive systems with AHA at different concentrations (Figure 29b, c, d) to check if we could improve plutonium retention with this complexant. We observed a slight improvement in plutonium retention using 0.1M ascorbic acid in 0.6 M HNO_3 and 0.3M AHA. However the plutonium retention never exceeded 35%. AHA was not working in the very oxidative environment created by the TBP/nitric acid complex in sc-CO_2. We therefore resorted to test oxalic acid, another complexant often used to bind to tetravalent actinides.

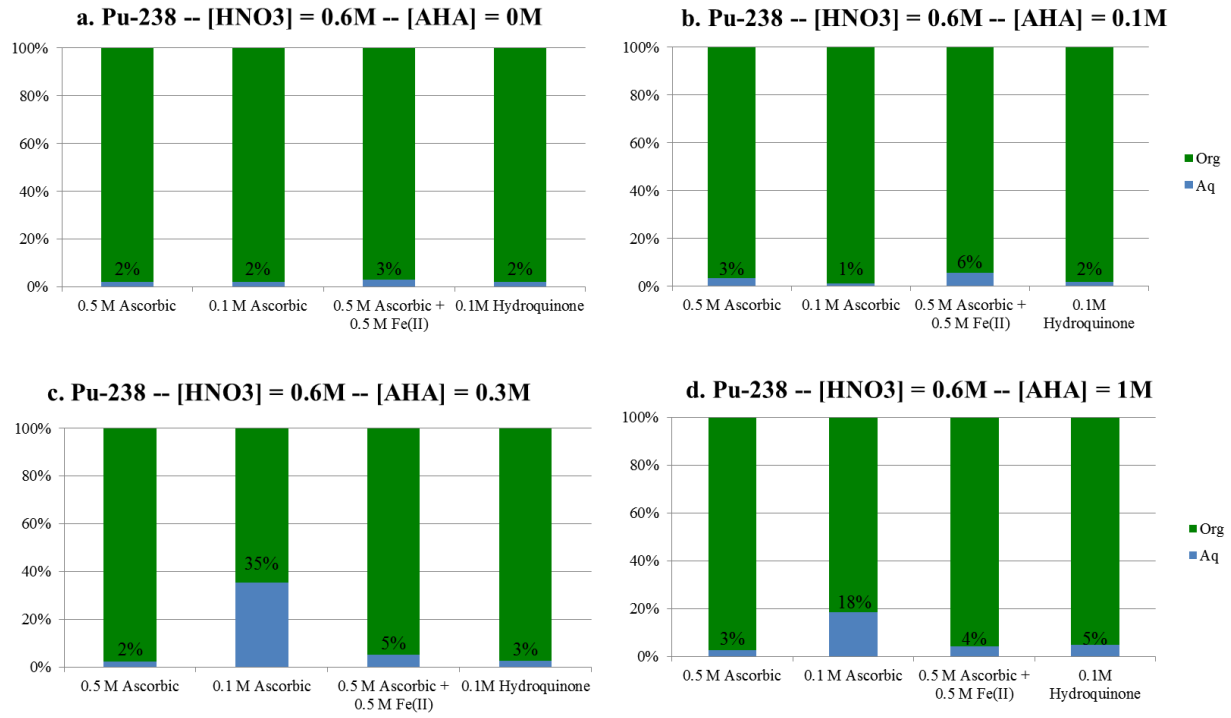

Figure 29. Plutonium partition between the aqueous phase (measured) and the organic phase (inferred) using different reducing agent and for different AHA concentrations in the aqueous phase.

8.2.2 Oxalic acid

First experiments with oxalic acid were done in batch contacts using tracers as described earlier.

Figure 30 shows the partition between the organic and the aqueous phase for different oxalic acid ($H_2C_2O_4 \cdot 2H_2O$) concentrations for plutonium (a) and uranium (b). Plutonium retention in the organic phase increases with the oxalic acid concentration while uranium extraction in the organic phase was not affected. A 76% plutonium retention was achieved using 0.5 M oxalic acid in 1.4 M HNO_3.

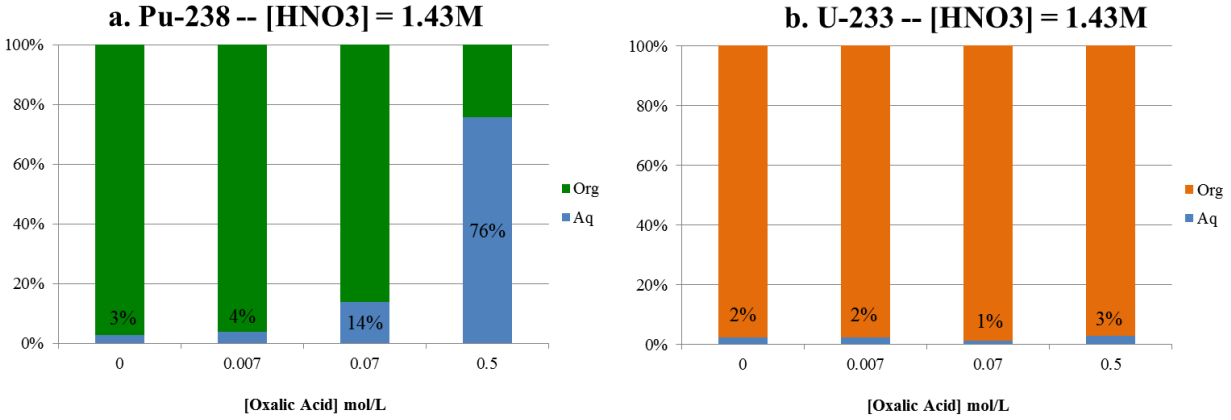

Figure 30. Plutonium (a) and uranium (b) partition between the aqueous phase (measured) and the organic phase (inferred) for different oxalic acid concentrations in the aqueous phase.

To confirm these promising results with our sc-CO_2 extraction system, we introduced 50 µL of a 60kdpm/mL actinide spike (U-233, Pu-239, Th-230, Np-237, Am-241) in HNO_3 (1.4 M) and oxalic acid (0.54M) solutions. We then extracted our analytes with TBP-HNO_3 1:1 (v/v) complex at 2900 PSI (~200atm) and 50°C. Figure 31 shows partition results between the two phases for this experiment. The experiment was not successful using 0.5 mL of aqueous solution. However, by using 2 mL of solution, oxalic acid was successful in retaining in the aqueous phase trivalents, tetravalent and pentavalent actinides (Pu, Am, Np) while allowing hexavalents (U) to be extracted into the CO_2 phase.

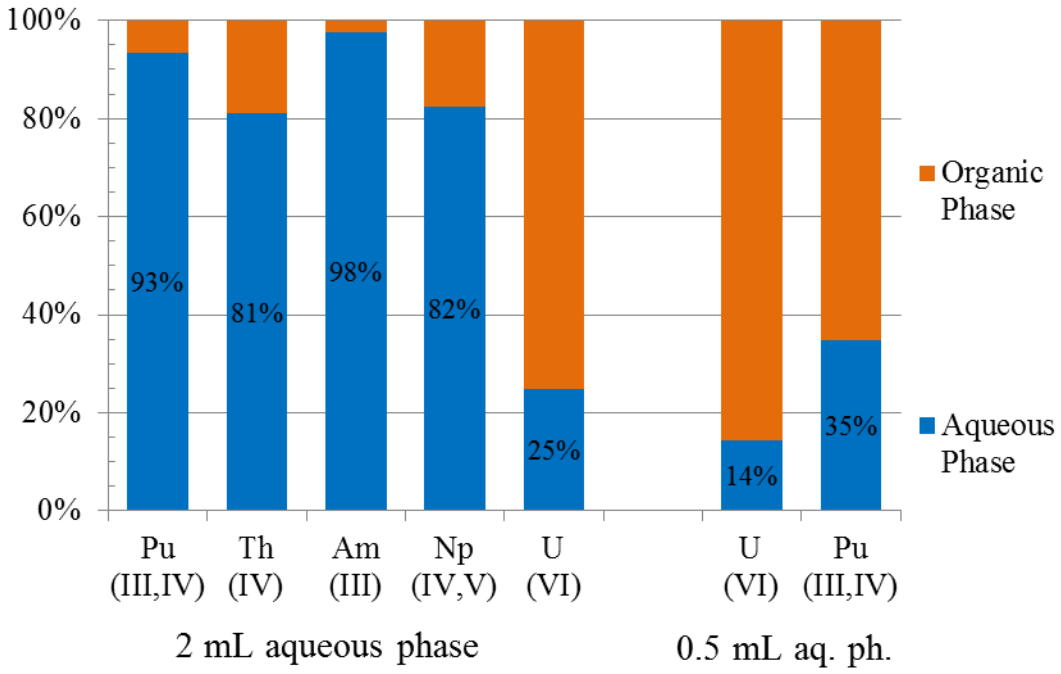

Figure 31. Actinide (Pu, Th, Am,Np, U) partition between the aqueous phase (measured) and the organic phase (inferred) for different volume of 0.54M oxalic acid in nitric acid (1.4M)

More experiments need to be done to fully understand the role of oxalic acid in this system and to be able to improve plutonium retention above 75%. The volume of the aqueous phase needs to be tuned, as well as the concentrations of oxalic acid and nitric acid. The amount of TBP used in the CO_2 phase needs also to be adjusted as well as the temperature and pressure of the fluid. This future work is the key to gain complete uranium selectivity using supercritical CO_2 as a solvent in this extraction scheme.

9. USING IONIC LIQUIDS AS A SEPARATION MEDIA

9.1 Introduction

The main research objective of this contract is to develop techniques for separation of uranium from lanthanides and other actinides using supercritical fluid carbon dioxide (sc-CO_2) as a solvent. Direct dissolution of uranium dioxide (UO_2) and lanthanide oxides (Ln_2O_3) in sc-CO_2 is well established in the literature.[14,16] The dissolution is typically carried out using a CO_2-soluble TBP-HNO_3 complex such

as $TBP(HNO_3)_{1.8}(H_2O)_{0.6}$ which converts UO_2 and Ln_2O_3 to $UO_2(NO_3)_2(TBP)_2$ and $Ln(NO_3)_3(TBP)_3$, respectively. Oxides of other actinides probably can also be dissolved in sc-CO_2 but have not been extensively studied. This supercritical fluid dissolution technique appears promising for nuclear waste management. However, little is known in the literature regarding separation of uranium from lanthanides and other actinides in sc-CO_2. This knowledge is essential for evaluating supercritical fluid-based technologies for reprocessing used nuclear fuel. For this PNNL contract, we have investigated the following two systems: (1) sc-CO_2 extraction of uranium in the presence of acetohydroxamic acid (AHA) and (2) separation of uranium from lanthanides using diglycolamide reagents.

1-butyl-3-methylimidazolium cation
bis(trifluoromethylsulfonyl)imide anion

$N(SO_2CF_3)_2^-$

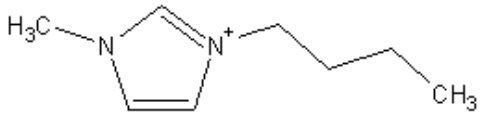

Figure 32. Structure of the ionic liquid [BMIM][Tf_2N]

9.2 Supercritical fluid extraction of uranium in the presence of AHA in ionic liquid

9.2.1 Stability of acetohydroxamic acid (AHA) in nitric acid solution

AHA is used in the UREX process for selective extraction of uranium from nitric acid solutions. We used Raman spectroscopy to investigate the stability of 0.5 M AHA in 3 M nitric acid as a function of time. Figure 22-b is the Raman spectrum of AHA in 3 M HNO_3. The symmetric vibrtional mode of AHA appears at ~ 960 cm^{-1} in the Raman spectra (Figure 33). When 0.5 M AHA is dissolved in 3 M HNO_3, AHA decomposes slowly to form acetic acid (CH_3COOH) probably according to the following reaction.

$$CH_3CONHOH + H_2O + H^+ \rightarrow CH_3COOH + NH_3OH^+$$

The appearance of the acetic acid peak at 892 cm^{-1} in 3 M HNO_3 was observed in 60 min (Figure 33-c) but not in 20 min (Figure 33-b). In Figure 33, we can clearly see that the intensity of AHA peak decreases while the intensity of acetic acid peak increases with time from 1h to 24 h (Figure 33spectra c to f). Within a short period of experimental time (e.g., 1 hr) in 3 M nitric acid, most of the added AHA should still be present in the acid solution for chemical reactions.

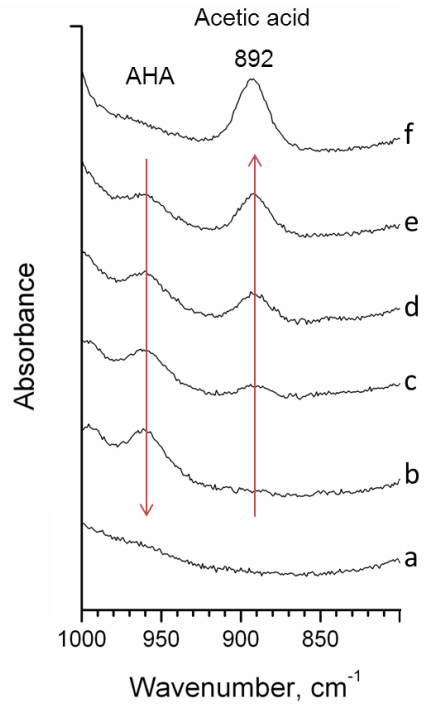

Figure 33. Raman Spectra of 0.5 M AHA in 3 M HNO_3 solution (a) 3 M HNO_3 blank, (b) 20 min with AHA, (c) 60 min, (d) 120 min, (e) 260 min, and (f) 24 hr.

9.2.2 Stability of AHA in ionic liquid

Acetohydroxamic acid is not soluble in ionic liquid [BMIM][Tf2N] but becomes soluble when the IL contains TBP(HNO3)1.8(H2O)0.6. The structure of the IL is given in Figure 32. With 0.5 M AHA in [BMIM][Tf2N] containing 16.7% TBP(HNO3)1.8(H2O)0.6, the IR spectra of the solution show that AHA slowly decomposes in the IL phase. In the first 2 hours, no acetic acid absorption peak was observed in the IR spectra (a and b in Figure 34). After 24 hours, the IR spectra of the IL solution showed the presence of acetic acid C=O peak at 1755 cm-1 and at 1721 cm-1 (spectra d and e in Figure 34). However, when UO2 was added to [BMIM][Tf2N] containing 16.7% TBP(HNO3)1.8(H2O)0.6 and 0.2 M AHA, decomposition of AHA to acetic acid occurred in 30 min as shown in spectra b and c in

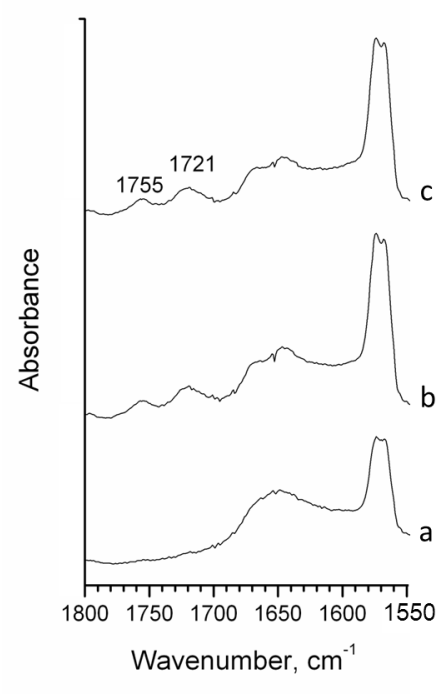

Figure 35. $TBP(HNO_3)_{1.8}(H_2O)_{0.6}$ is known to cause oxidation of UO_2 to $(UO_2)^{2+}$ followed by subsequent formation of $UO_2(NO_3)_2(TBP)_2$. It is possible that during the oxidation process some nitrogen-containing species are produced which could cause decomposition of AHA.

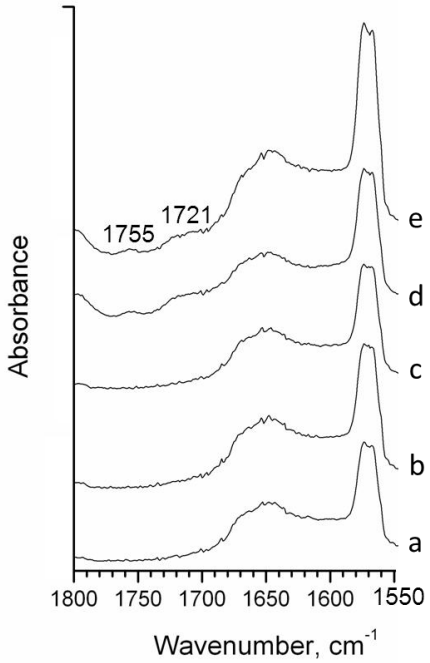

Figure 34. FTIR spectra of 0.5 M AHA dissolved in $[BMIM][Tf_2N]$ containing 16.7% $TBP(HNO_3)_{1.8}(H_2O)_{0.6}$ (a) beginning, (b) 1 hr, (c) 2 hr, (d) 24 hr, and (e) 48 hr.

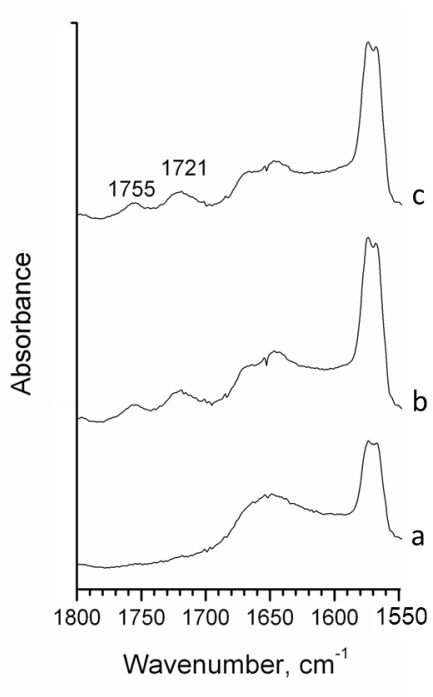

Figure 35. (a) 0.1 M AHA dissolved in IL containing 16.7% $TBP(HNO_3)_{1.8}(H_2O)_{0.6}$ with UO_2, beginning FTIR spectrum (b) at 30 min (c) at 120 min.

9.2.3 Dissolution of UO_2 in IL containing AHA

The experimental procedure for direct dissolution of UO_2 in [BMIM][Tf_2N] containing $TBP(HNO_3)_{1.8}(H_2O)_{0.6}$ and 0.1 M AHA is described as follows: (1) 600 µL of $TBP(HNO_3)_{1.8}(H_2O)_{0.6}$ was added to 3 mL of [BMIM][Tf_2N] in a 8 mL glass vial and subjected to continuous stirring at room temperature and (2) 26.2 mg of UO_2 and 0.1 M AHA were then added to the solution. The dissolution process was monitored by acquiring UV/Vis spectra of the IL phase at different times as shown in Figure 36. About 45% of the added UO_2(s) dissolved in the IL phase in the first hour and 35% more dissolved in the second hour. The rate of dissolution of UO_2 in [BMIM][Tf_2N] with $TBP(HNO_3)_{1.8}(H_2O)_{0.6}$ at room temperature depends on the stirring speed of the magnetic stirrer. Between 900 and 1200 rpm, the dissolution rate of UO_2 in this IL system reaches near a constant under our experimental conditions. Therefore, the UO_2 dissolution experiments were carried out at a stirring speed of 1200±10 rpm.
The initial rate of dissolution of UO_2 in the IL (Figure 36) increases exponentially and resembles first order kinetics. A plot of $\ln[(A_\infty - A)/A_\infty]$ versus time is shown in Figure 37, where A is the absorbance at time t and A_∞ is taken as the absorbance at 300 min. The absorption of the uranyl species in the IL at 424 nm is used in this plot. The slope of the $\ln[(A_\infty - A)/A_\infty]$ versus time plot, is 0.0093 min^{-1} (or $t_{½}$ = 74.5 min), which may be regarded as the rate constant of the initial pseudo first-order dissolution process for UO_2 in the IL with AHA. Without AHA, the UO_2 dissolution rate is about 3 times faster. The slower dissolution rate is probably caused by AHA interaction with the TBP-HNO_3 complex.

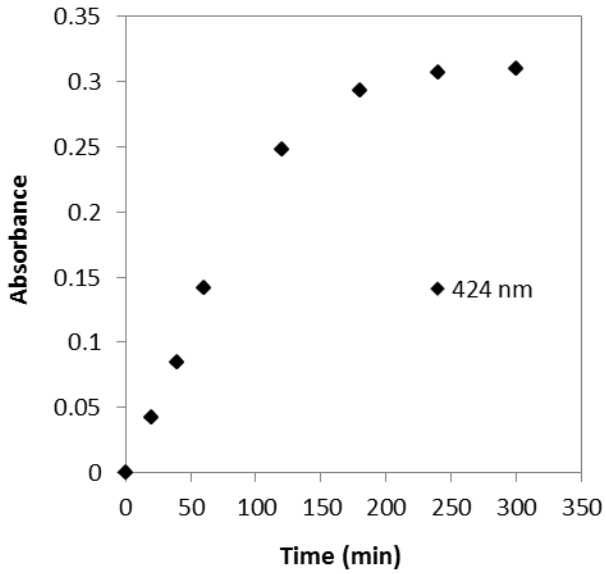

Figure 36. Rate of dissolution of UO_2(s) in [BMIM][Tf_2N] with $TBP(HNO_3)_{1.8}(H_2O)_{0.6}$ (16.7% by volume) and AHA (0.1 M) at room temperature (absorbance versus dissolution time (min) for peak at 424 nm).

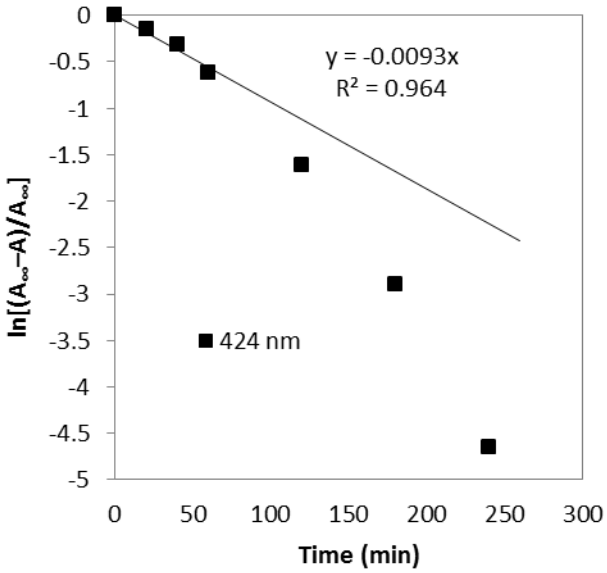

Figure 37. Plot of $\ln[(A_\infty - A)/A_\infty]$ versus time for the dissolution of UO_2 in [BMIM][Tf2N] containing $TBP(HNO_3)_{1.8}(H_2O)_{0.6}$ and 0.1 M AHA

9.2.4 Sc-CO_2 extraction of uranyl complex from IL solution containing AHA

In this experiment, we took 1 mL of an IL solution containing 16.7% (v/v) $TBP(HNO_3)_{1.8}(H_2O)_{0.6}$, 0.1 M AHA and 0.1 M uranium and then added another 30% (v/v) TBP in the reaction cell for sc-CO_2 extraction. Figure 38 shows that the time required to reach a steady state for uranium extraction is about 30 min. The UV/Vis absorption spectra of the uranyl complex removed from the supercritical fluid phase is identical to that of $UO_2(NO_3)_2(TBP)_2$. The extraction efficiency of $UO_2(NO_3)_2(TBP)_2$ is greater than 92 % for 30 min static extraction followed by 2.5 h dynamic extraction including depressurization (flow rate: 0.3-0.4 mL/min). The percentage of extraction was estimated using a calibration curve of absorptions of different concentrations of $UO_2(NO_3)_2(TBP)_2$ in UV/Vis spectra.

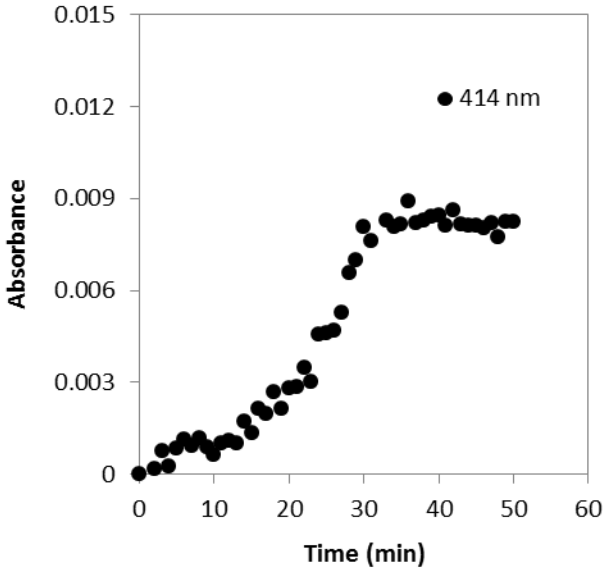

Figure 38. Static extraction of 0.1 M UO_2 solution containing 16.7 % $TBP(HNO_3)_{1.8}(H_2O)_{0.6}$, 0.1 M AHA and 30% (v/v) TBP from IL phase into sc-CO_2 phase at 40 ^oC and 200 atm.

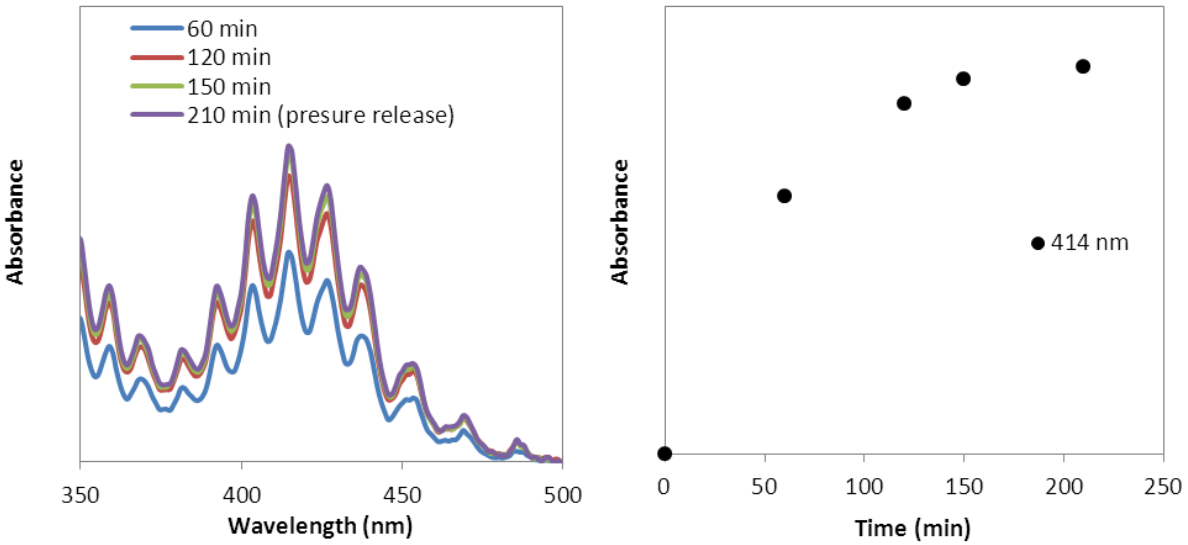

Figure 39. (a) UV/Vis spectra of the hexane trap solution - spectrum feature is identical to that of $UO_2(NO_3)_2(TBP)_2$, (b) plot of absorbance (uranyl peak at 414 nm in the hexane trap solution) versus time during dynamic extraction.

9.2.5 Sc-CO_2 extraction of uranium from nitric acid solution containing AHA

In this experiment, we placed 1 mL of 0.1 M $UO_2(NO_3)_2 \cdot 6H_2O$ in 3M nitric acid solution containing 0.1 M AHA and 30% (v/v) TBP in the reaction cell for sc-CO_2 extraction at 40 ^oC and 200 atm. A steady state of uranium extraction was reached in a very short time (within 3 min) as shown in Figure 40. The extraction efficiency of $UO_2(NO_3)_2(TBP)_2$ in this case is about 62 % for 2.5 h dynamic extraction and depressurization (Figure 41).

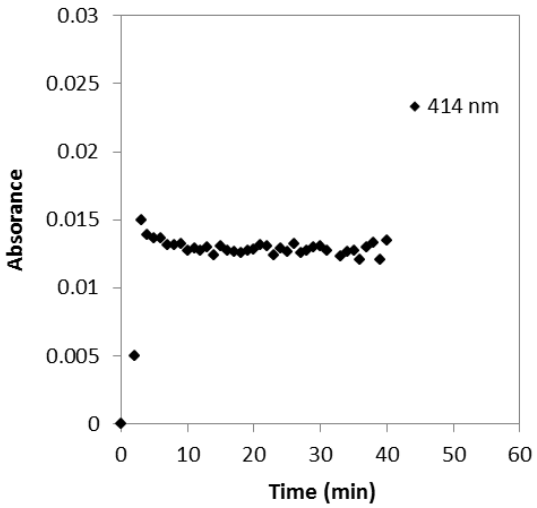

Figure 40. Static extraction of 0.1 M $UO_2(NO_3)_2$. $6H_2O$ in 3M HNO_3 solution containing 30% (v/v) TBP and 0.1 M AHA from the aqueous phase into sc-CO_2 phase at 40 °C and 200 atm.

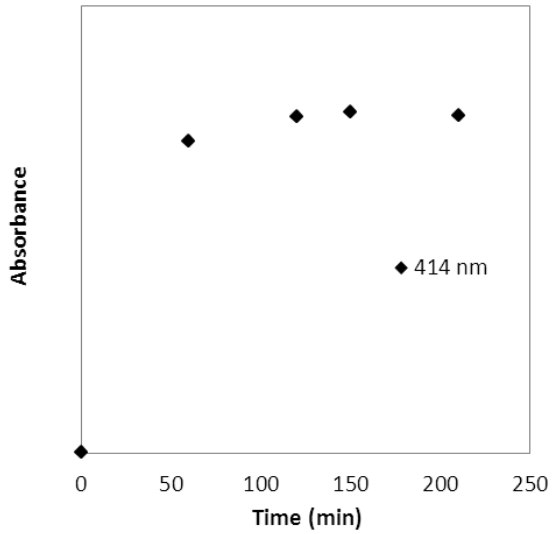

Figure 41. Plot of absorbance versus dynamic extraction time for 5 mL hexane trap solution monitored at 414 nm.

9.3 Supercritical fluid extraction and separation of $(UO_2)^{2+}$ and Nd^{3+} complexes from IL with diglycolamide

In this study, we first prepared an IL solution containing 0.15 M $UO_2(NO_3)_2(TBP)_2$ and 0.15 M $Nd(NO_3)_3(TBP)_3$ by dissolving appropriate amounts of UO_2 and Nd_2O_3 in [BMIM][Tf_2N] with $TBP(HNO_3)_{1.8}(H_2O)_{0.6}$. Sc-$CO_2$ extraction of the uranyl and neodymium complexes from the IL phase was performed using a fiber-optic cell with a CCD-array UV-Vis spectrometer. Based on the in situ spectroscopic data, the amount of $Nd(NO_3)_3(TBP)_3$ dissolved in the sc-CO_2 phase was found less than that of $UO_2(NO_3)_2(TBP)_2$ as showed in Figure 42. If extra 30% (v/v) of TBP is added to the IL solution, the solubilities of both $UO_2(NO_3)_3(TBP)_3$ and $Nd(NO_3)_3(TBP)_3$ in the sc-CO_2 phase could be increased but the time required to reach a steady state is longer (Figure 43).

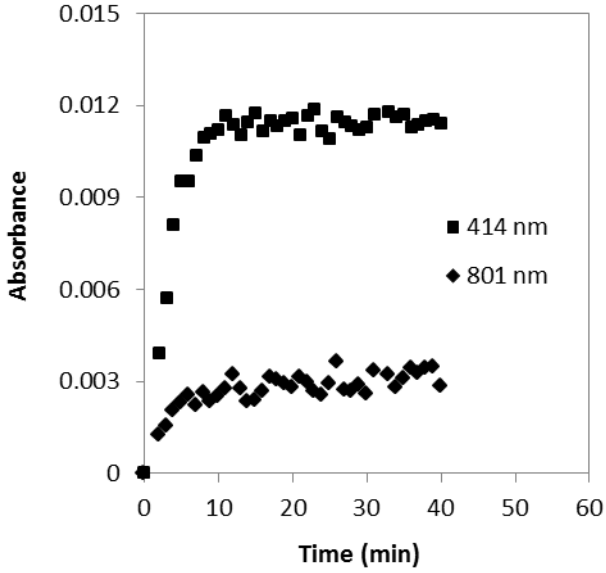

Figure 42. Static extraction of a mixture of 0.15 M $UO_2(NO_3)_2(TBP)_2$ and 0.15 M $Nd(NO_3)_3(TBP)_3$ from IL phase into sc-CO_2 phase (without extra TBP) at 40 ^oC and 200 atm.

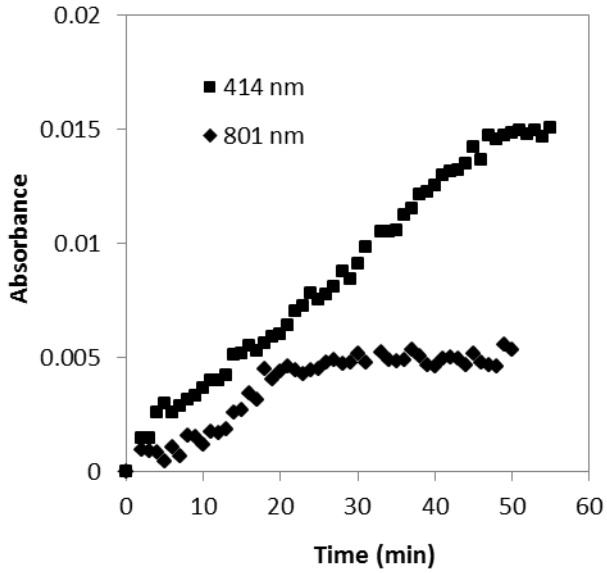

Figure 43. Static extraction of a mixture of 0.15 M $UO_2(NO_3)_2(TBP)_2$ and 0.15 M $Nd(NO_3)_3(TBP)_3$ from IL phase into sc-CO_2 phase (with 30% TBP) at 40 ^oC and 200 atm.

Diglycolamides such as TBDGA (N,N,N',N'-tetrabutyldiglycolamide) are known to form stable complexes with uranyl ions $(UO_2)^{2+}$ and with lanthanide ions Ln^{3+} in ionic liquids.[17,17,18] TBDGA forms a 1:2 complex with $(UO_2)^{2+}$ and a 1:3 complex with Nd^{3+}. Because TBDGA is a neutral ligand, its complexes with $(UO_2)^{2+}$ and with Nd^{3+} are charged. These charged TBDGA complexes are soluble in IL and are not extractable by sc-CO_2. The $Nd(TBDGA)_3^{3+}$ complex is probably more stable than the $(UO_2)(TBDGA)_2^{2+}$ complex in IL. Our idea is to test the feasibility of separating $UO_2(NO_3)_2(TBP)_2$ and $Nd(NO_3)_3(TBP)_3$ in sc-CO_2 by contacting with an IL containing TBDGA.

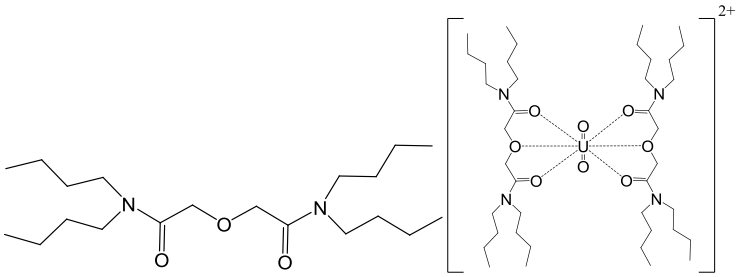

Figure 44. Structure of TBDA and its complex with uranyl ions.

Our experimental results indicate that when TBDGA is added to a [BMIM][Tf_2N] solution containing a mixture of $UO_2(NO_3)_2(TBP)_2$ and $Nd(NO_3)_3(TBP)_3$, the relative amounts of the uranyl and the neodymium complexes extracted into the sc-CO_2 phase can be significantly altered depending on the concentration of TBDGA present in the IL solution. Table 7 summarizes the results of separation of uranium from neodymium using TBDGA as a competing ligand in a sc-CO_2-IL biphasic system. The separation factor of $(UO_2)^{2+}/Nd^{3+}$ can be increased from ~3 (without TBDGA) to >74.9 when the mole ratio of $(UO_2)^{2+}$: Nd^{3+}: TBDGA = 1: 1: 1.25. Under this condition, Nd^{3+} is virtually not extractable by sc-CO_2. Based on this result, we think separation of uranium and lanthanides in the sc-CO_2-TBP-HNO_3 system is possible using diglycolamide as a competing ligand in contact with an IL phase.

Table 7. Dynamic extraction of uranyl and neodymium complex from ionic liquid phase into a hexane trap solution using sc-CO_2 with/without TBP at 200 atm and 40 ℃.

	% Extraction		
sc-CO_2 modifier	UO_2^{2+} (414 nm)	Nd^{3+} (801 nm)	UO_2^{2+}/ Nd^{3+}
[a] Neat CO_2	68.9 ± 6.2	20.2 ± 2.3	3.4
[b] 30% TBP	> 99	28.2 ± 3.5	3.2
[c] 30% TBP + TBDGA (UO_2^{2+}: Nd^{3+}: TBDGA =1: 1: 0.5)	87.5 ± 2.7	15.0 ± 1.3	6.4
[c] 30% TBP + TBDGA (UO_2^{2+}: Nd^{3+}: TBDGA =1: 1: 1)	79.0 ± 5.0	5.8 ± 0.8	14.2
[c] 30% TBP + TBDGA (UO_2^{2+}: Nd^{3+}: TBDGA =1: 1: 1.25)	74.9 ± 4.7	< 1	> 74.9

[a] Experimental condition: 30 min static extraction and 3 h dynamic extraction (flow rate 0.3-0.4 mL/min) including depressurization. [b] Experimental condition: 60 min static extraction and 2.5 h dynamic extraction (flow rate 0.3-0.4 mL/min) including depressurization. [c] Experimental condition: 30 min static extraction and 2.5 h dynamic extraction (flow rate 0.3-0.4 mL/min) including depressurization.

10. CONCLUSIONS

This report shows results obtained by PNNL and the University of Idaho on the selective dissolution of uranium. We started with a background overview on the project goals and on supercritical fluids and their ability to extract uranium. Then the characteristics of the different uranium oxides (UO_2, UO_3, U_3O_8) used in our extraction system were reported. This characterization was essential to calibrate the UV-Vis online monitoring spectrometer in order to assess $UO_2(NO_3)_2(TBP)_2$ complex solubility and determine uranium extraction efficiencies of the different oxides in sc-CO_2. We also demonstrated the back-extraction of uranium into an aqueous phase using ammonium carbonate solutions. Then we showed some promising results on the selective extraction of uranium. We were able to inhibit plutonium and neptunium co-extraction using oxalic acid as a complexing agent to tetravalent actinides. This will reduce proliferation risks by leaving plutonium with the fission products while minimizing the amount of HLW. Finally, results from the University of Idaho, including the use of ionic liquids as a supportive media for the selective extraction of lanthanides and actinides, were presented.

This report closes the proof of concept phase for the selective extraction of uranium from liquid or supercritical carbon dioxide. We were successful in demonstrating uranium extraction into supercritical fluids, and its back extraction and recovery as uranium oxide. We also showed the selectivity of this method for uranium, by inhibiting plutonium and neptunium co-extraction with uranium. Finally we showed that we could also use ionic liquids as a supporting media for the separations. This technology has low environmental impact and would enable sustainable fuel cycles by greatly reducing the amount of liquid waste generated.

In the future, we would like to get a more fundamental understanding of the chemistry, thermodynamics and kinetics involved with this technology. We would like to use this knowledge to fully optimize our extraction and back extraction systems and the chemistry involved. We also would like to test this method with fission products and lanthanides and demonstrate the feasibility of a scale-up system by using plutonium oxides.

ACKNOWLEDGEMENTS

Cyndi Niver, technician at PNNL worked on the SFE system and was instrumental to this project.

Natasha Pence, from The College of Idaho worked on the project for two months this summer as a DOE intern under the Undergraduate Laboratory Internship (SULI) program. Natasha helped this project by running experiments in the lab and by analyzing data. She gained a lot of experience during her internship and is on her way to become part of the next generation of radiochemists.

This work was funded by DOE's Nuclear Energy Fuel Cycle R&D program and was done at Pacific Northwest National Laboratory (PNNL). PNNL is operated by Battelle for the DOE. PNNL subcontracted some of this work to the University of Idaho, under the direction of Chien M. Wai.

REFERENCES

1. Barelko E. V. and Solyanina I. P. "Radiolysis of solutions of TBP in contact with nitric acid." *Atomic Energy* **1973**. 35(4): 898-902.
2. Enokida Y., Tomioka O., Lee S.-C., Rustenholtz (Farawila) A., Wai, C. M. "Charact. of a Tri-n-butyl Phosphate-Nitric Acid Complex: a CO_2-Soluble Extractant for Dissolution of U. Dioxide". *Ind. Eng. Chem. Res.* **2003**. 42(21), 5037—5041
3. Anne F. Rustenholtz-Farawila, Ph.D. Thesis. Supercritical Fluid Extraction: Spectroscopic Study of Interactions Comparison to Solvent Extraction. P.144 **2005**. http://tel.archives-ouvertes.fr/docs/00/04/82/05/PDF/tel-00009652.pdf
4. Samsonov M.D., Wai C. M., Lee S.-C., Kulyako, Y., Smart, N.G. Dissolution of uranium dioxide in supercritical fluid carbon dioxide. *Chem. Comm*. **2001**. 1868—1869
5. Rao A., Kumar P., Ramakumar K.L. Separation of uranium from different uranium oxide matrices employing supercritical carbon dioxide extraction. *J. Radioanal. Nucl. Chem.* **2010**. 285, 247—257
6. Wai C.M. "Emerging green separation techniques for nuclear waste management", *ACS Symposium Series Book 1046*, Eds. C.M. Wai, B.J. Mincher, American Chemical Society, Washington, DC, **2010**. Chapter 5, p. 53-63
7. Carrot M.J., Waller B.E., Smart N.G., Wai C.M. "High solubility of $UO_2(NO_3)_2 \cdot 2TBP$ complex in supercritical CO_2" *Chem Commun*. **1998**. 373-374
8. Shimada T., Ogumo S., et al. "Selective Extraction of Uranium from a Mixture of Metal or Metal Oxides by a Tri-n-butylphosphate Complex with HNO_3 and H_2O in Supercritical CO_2." *Anal. Sci.* **2006**. 22(11): 1387-1391.
   Kamiya M., Miura S., Sano Y., Koyama T. "Development of Actinides Co-extraction System with Direct Extraction
9. Pelikan P., Ceppan M., Liska M. "Applications of numerical methods in molecular spectroscopy", *CRC press* **1994**
10. Baumgaertner F., Finsterwalder L. "On the Transfer Mechanism of Uranium(VI) and Plutonium(IV) Nitrate in the System Nitric Acid-Water/Tributylphosphate-Dodecane", *J. Phys. Chem*., **1970**, 74 (1), 108–112.
11. Blanco R. E., Blake C. A., Jr., Davis W., Jr, Rainey R. H. "Survey of Recent Developments in Solvent Extraction with TBP" *Symposium on Aqueous Reprocessing Chemistry*, **1963.**
12. Peper Shane M., Brodnax Lia F., Field Stephanie E., Zehnder Ralph A. Valdez Scott N., Runde Wolfgang H. "Kinetic Study of the Oxidative Dissolution of UO2 in Aqueous Carbonate Media" *Ind. Eng. Chem. Res*. **2004**, 43, 8188-8193.
13. Iso S., Uno S., Meguro Y., Sasaki T., Yoshida Z. "Pressure dependence of extraction behavior of plutonium(IV) and uranium(VI) from nitric acid solution to supercritical carbon dioxide containing tributylphosphate" *Progress in Nuclear Energy*, **2000**, 37(1-4), 423-428.
14. Tkac Peter, Paulenova Alena "The Effect of Acetohydroxamic Acid on Extraction and Speciation of Plutonium" *Separation Science and Technology*, **2008**, 43: 2670–2683.
15. Samsonov, M. D.; Wai, C. M.; Lee, S. C.; Kulyako, Y.; Smart, N. G., *Chem. Commun.* **2001**, 1868-1869.
16. Tomilka, O.; Enokida, Y.; Yamamoto, I. *Separation Science & Technology* **2002**, *37*, 1153-1162.
17. Shimojo, K.; Kurahashi, K.; Naganawa, H. *Dalton Trans.* **2008**, 5083-5088.
18. Shen, Y.L.; Tan, X.W.; Wang, I.; Wu, W.S. *Sep. Purif. Technol.* **2011**, *78*, 298-302.

Appendix A. ICP-OES results for uranium oxide analysis

		Run Date >	2/15/2012	2/15/2012	2/15/2012	2/15/2012	2/15/2012	2/15/2012
		Multiplier >	1.0	1.0	1.0	1.0	1.0	1.0
		RPL/LAB >	405 diluent	12-0602	12-0603	12-0604	12-0604 rep	12-0605
Instr. Det. Limit (IDL)	Est. Quant. Limit (EQL)	Client ID >	Lab diluent	Blank	UO2	UO3		U3O8
(µg/mL)	(µg/mL)	(Analyte)	(µg/mL)	(µg/mL)	(µg/mL)	(µg/mL)	(µg/mL)	(µg/mL)
0.0290	0.290	U	-	-	360	530	536	371
Other Analytes								
0.0026	0.026	Ag	-	-	-	-	-	-
0.0064	0.064	Al	-	0.298	0.306	0.307	0.307	0.355
0.0480	0.480	As	-	-	-	-	-	-
0.0034	0.034	B	[0.032]	3.48	3.94	4.46	4.52	4.49
0.0003	0.003	Ba	-	[0.0016]	-	-	-	-
0.0001	0.001	Be	-	-	0.0068	0.0099	0.0102	0.0072
0.0200	0.200	Bi	-	-	-	-	-	-
0.0120	0.120	Ca	-	[0.074]	[0.062]	0.282	0.286	[0.091]
0.0011	0.011	Cd	-	-	-	-	-	-
0.0130	0.130	Ce	-	-	-	-	-	-
0.0013	0.013	Co	-	-	-	-	-	-
0.0024	0.024	Cr	-	-	0.252	0.365	0.352	0.255
0.0027	0.027	Cu	-	-	-	-	-	-
0.0016	0.016	Dy	-	-	-	-	[0.0018]	[0.0032]
0.0012	0.012	Eu	-	-	-	-	-	-
0.0010	0.010	Fe	-	0.0214	0.0284	0.149	0.144	0.0921
0.0390	0.390	K	-	[0.33]	0.464	0.792	0.773	0.425
0.0009	0.009	La	-	[0.0010]	0.0446	0.0577	0.0604	0.0422
0.0006	0.006	Li	[0.0007]	[0.0035]	0.0095	0.0608	0.0618	0.0279
0.0012	0.012	Mg	-	-	-	-	-	-
0.0003	0.003	Mn	-	-	0.0121	0.0210	0.0203	0.0166
0.0040	0.040	Mo	-	-	-	-	-	0.187
0.0051	0.051	Na	-	4.18	5.05	5.57	5.68	5.46
0.0051	0.051	Nd	-	-	-	[0.015]	-	-
0.0040	0.040	Ni	-	-	[0.018]	[0.020]	[0.016]	[0.023]
0.0890	0.890	P	-	-	-	-	-	-
0.0220	0.220	Pb	-	-	[0.035]	[0.085]	[0.039]	[0.062]
0.0074	0.074	Pd	-	-	-	-	-	-
0.0130	0.130	Rh	-	-	-	-	-	-
0.0043	0.043	Ru	-	-	-	-	-	-
0.0910	0.910	S	-	-	-	-	-	-
0.0320	0.320	Sb	-	-	-	-	-	-
0.0720	0.720	Se	-	-	-	-	-	-
0.0093	0.093	Si	-	0.983	1.18	1.08	1.06	0.992
0.0160	0.160	Sn	-	-	-	-	-	-
0.0001	0.001	Sr	-	[0.0005]	0.0015	0.0023	0.0024	0.0016
0.0160	0.160	Ta	-	-	-	-	-	-
0.0110	0.110	Te	-	-	-	-	-	-
0.0043	0.043	Th	-	-	1.67	2.44	2.42	1.70
0.0008	0.008	Ti	-	[0.0021]	0.0232	0.0338	0.0339	0.0267
0.0180	0.180	Tl	[0.039]	-	-	-	-	[0.028]
0.0010	0.010	V	[0.0013]	[0.0030]	-	-	-	[0.0039]
0.0110	0.110	W	-	-	[0.016]	[0.024]	[0.039]	-
0.0002	0.002	Y	-	-	-	-	-	-
0.0021	0.021	Zn	-	[0.0041]	[0.0023]	[0.013]	[0.017]	[0.012]
0.0009	0.009	Zr	-	[0.0032]	-	-	-	-

1) "0" indicates the value is < MDL. The method detection limit (MDL) = IDL times the "multiplier" near the top of each column. The estimated sample quantitation limit = EQL (in Column 2) times the "multiplier". Overall error for values ≥ EQL is estimated to be within ±15%.

2) Values in brackets [ ] are ≥ MDL but < EQL, with errors likely to exceed 15%.

Appendix B. Molar Extinction Coefficient (ε) at 414 nm Determination at 50°C for Different Pressure Settings

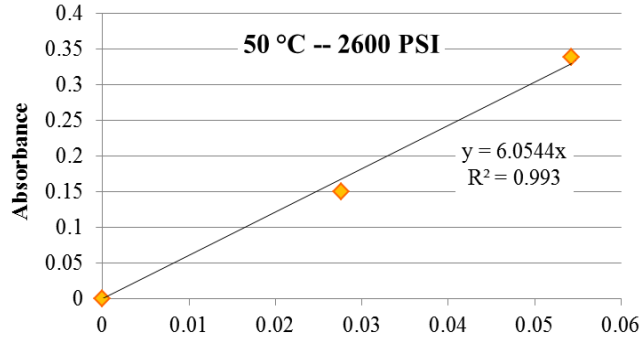

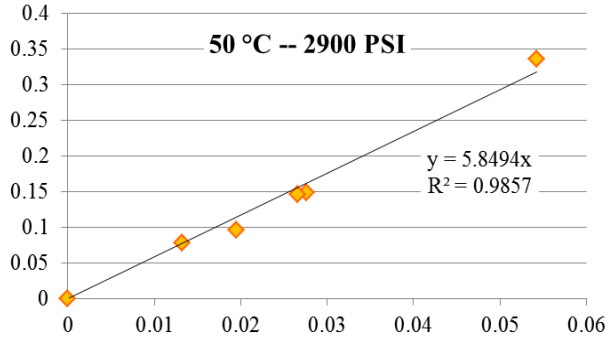

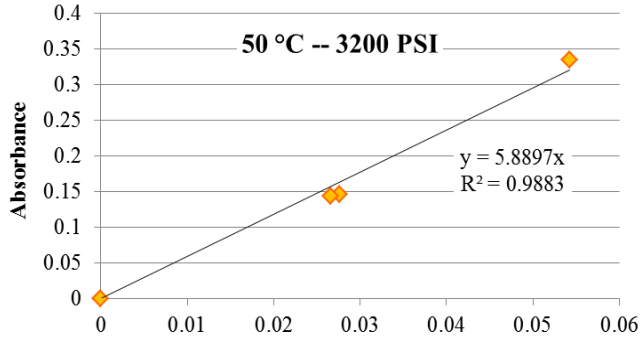

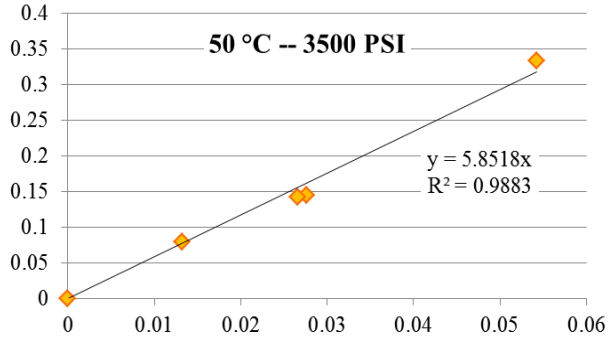

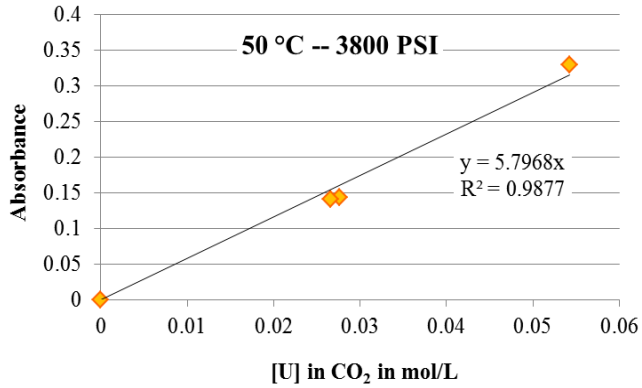

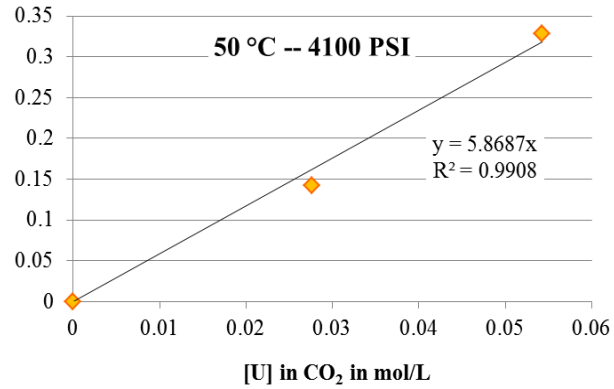

Appendix C. Molar Extinction Coefficient (ε) at 414 nm Determination at 40°C and 60°C for Different Pressure Settings

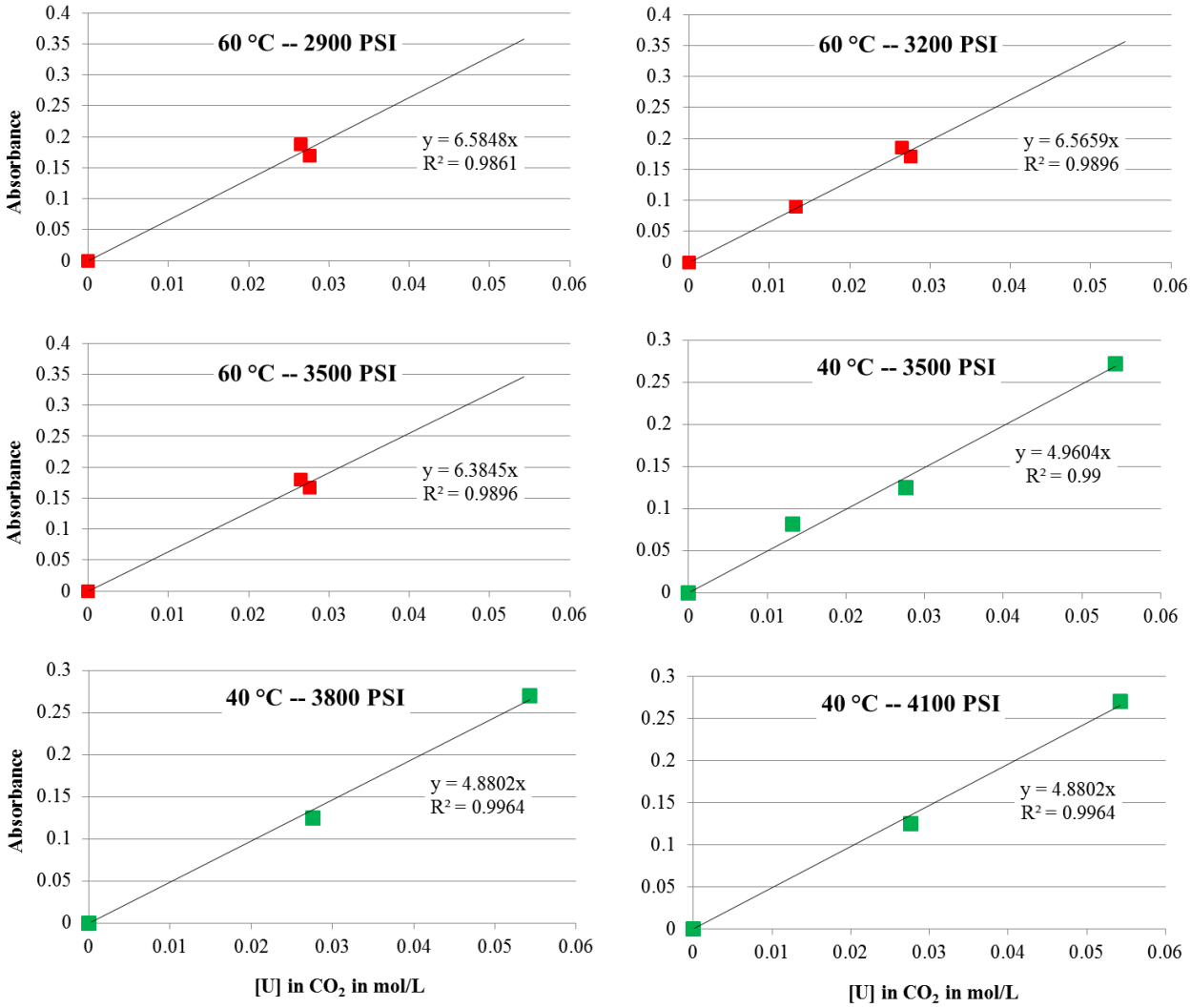

Appendix D. Molar Extinction Coefficient (ε) at 414 nm Determination at 25°C for Different Pressure Settings